The Islamic University of Gaza
Deanery of Graduate Studies
Faculty of Engineering
Electrical Engineering Department


# DESIGN AND IMPLEMENTATION OF "AN EXPERIMENTAL SEGWAY MODEL"

**By**

**Wael A. M. Younis**

**Supervisor**

**Prof. Dr. Muhammed Abdelati**

"A Thesis Submitted in Partial Fulfillment of the Requirements for the

Degree of Master of Science in Electrical Engineering."

1430 - 2009

# Abstract

The segway is the first transportation product to stand, balance, and move in the same way as human. It is a truly 21st-century idea. The aim of this research is to study the theory behind building segway vehicles based on the stabilization of an inverted pendulum. An experimental model has been designed and implemented through this study. The model has been tested for its balance by running a Proportional Derivative (PD) algorithm on a microprocessor chip. The model has been identified in order to serve as an educational experimental platform for segways.

**عنوان البحث باللغة العربية:**

## تصميم وتنفيذ نموذج مخبري للـــ "سيغواي"

**ملخص البحث بالعربية:**

تعتبر الـــ "سيغواي" أول وسيلة تنقل تحاكي الإنسان في عملها مـــن حيـــث الوقـــوف والاتـــزان والحركة. يهدف هذا البحث لدراسة الجوانب النظرية لتصميم الـــ "سيغواي" اعتماداً على مبدأ عمل البندول المقلوب. من خلال هذه الدراسة تم تصميم وتنفيذ نموذج مخبري للـــ "ســـيغواي" وقـــد تـــم التحكم في اتزانه من خلال تنفيذ متحكم نوع (بي دي) تم تنفيذه بواسطة المتحكم الـــدقيق. هـــذا النموذج قد تم تجهيزه ليخدم كنموذج تعليمي مخبري بهدف دراسة الـــ "سيغواي.

# Dedication

***To all my family members who have been a constant source of motivation, inspiration, and support.***

# Acknowledgements

I would like to express my sincere thanks to the many people who have contributed to the success of this research, in particular my thesis supervisor, Prof. Dr. Muhammed Abdelati, for his support, encouragement and professional assistance throughout the work of this research.

Special thanks to all other Islamic University staff members that I may have called upon for assistance especially Dr. Mohammed T. Hussein and Dr. Mohammed Alhnajouri, as their suggestions have helped with the development of this thesis.

I would like to also extend my gratitude to my family for the support they have given me.

I would like to thank the Islamic University of Gaza for accepting me in its graduate program and motivated me to do this work.

# Nomenclature

| | |
|---|---|
| ADC | Analog to Digital Converter |
| BJT | Bbipolar junction Transistor |
| DC | Direct Current |
| DIR | Direction |
| DLP | Digital Light Processing |
| DMD | Digital Micromirror Device |
| DSP | Digital Signal Processing |
| EMF | Electro Motive Force |
| HT | Human Transporter |
| HTV | Human Transport Vehicle |
| IC | Integrated Circuit |
| IMOD | Interferometric modulator display |
| IR | Infra-Red |
| LED | Light Emitting Diode |
| LHS | Left Half Side |
| MEMS | Micro Electro Mechanical Systems |
| MIPS | Millions of Instructions Per Second |
| MOSFET | Metal Oxide Semiconductor Field Effect Transistor |
| MST | Micro System Technology |
| NiCad | Nickel Cademium |
| PC | Personal Computer |
| PCB | Printed Circuit Board |
| PID | Proportional Integral Derivative |
| PWM | Pulse Width Modulation |
| RHS | Right Half Side |
| SISO | Single Input Single Output |
| SLA | Sealed Lead Acid |
| $x$ | Distance (m) |
| $\dot{x}$ | Speed (m/s) |
| $\ddot{x}$ | Acceleration ($m/s^2$) |
| $\varphi$ | Error angle (rad) |
| $\dot{\varphi}$ | Error angular speed (rad/s) |
| $\ddot{\varphi}$ | Error angular acceleration ($rad/s^2$) |

| | |
|---|---|
| $k_e$ | Constant of the motor's back-EMF (Vs/rad) |
| $l$ | Length of the pendulum (m) |
| $r$ | Wheel radius (m) |
| $R$ | Resistance of the Motor ($\Omega$) |
| $M_p$ | Mass of the pendulum (kg) |
| $I_p$ | Moment of inertia of the pendulum (kg.m$^2$) |
| $M_w$ | Mass of the wheel (kg) |
| $I_w$ | Inertia of the wheel (kg.m$^2$) |
| $g$ | Acceleration of gravity (m/s$^2$) |

# Contents

# List of Tables

# List of Figures

# Chapter 1

# Introduction and Literature Review

## 1.1 Research Motivation and Goal

Dean Kamen, inventor and entrepreneur, first penned the idea of a revolutionary new type of personal transportation during the mid 1990s. Nowadays, his invention, the Segway Human Transporter (HT), is a common sight in America and is sold around the world. The Segway HT is a vehicle which has two coaxial wheels driven independently by a controller that balances the vehicle both with and without a rider. The balancing is regulated by feedback from an array of tilt sensors and gyroscopes. The control system must be robust enough to accept riders of different weights and responsive enough to provide adequate balancing for different riders and riding styles.

The aim of this research is to study the theory behind building a self-balancing vehicle that functions similarly to the Segway Human Transporter (HT) segway vehicle based on the stabilization of an inverted pendulum. An experimental model has been designed and implemented through this study (Figure 1.1). The model has been tested for its balance by running a Proportional Integral Derivative (PID) algorithm on a microprocessor chip. The model has been identified in order to serve as an educational experimental platform for segways. This work focuses on the problem of an inverted pendulum on a two-wheeled vehicle for human transportation, where the person riding the vehicle acts as pendulum. The forward movement is caused by the rider's inclination with respect to the equilibrium position.

Angular feedback from a gyroscopic sensor and PWM output to motors is used in a control system to achieve balance of the vehicle. The process goes through to self balance is similar to how a human being balance. The human brain recognizes the force due to gravity on the vestibular system and is able to discern the direction it is coming from. The brain then sends impulses to the muscles in the limbs to help provide balance. Similarly, the microcontroller receives information from sensors, interprets the information and then sends commands to the drive system to maintain balance. This microcontroller communicates with a PC, allowing collection of relevant vehicle data for analysis.

Figure 1.1: General view of the vehicle.

## 1.2 Literature Review

This section provides an overview of previous efforts to construct self-balancing devices. The knowledge gained in reviewing these endeavors was extremely useful in the preliminary design of our Segway.

### 1.2.1 The Segway Model, 2002

The Segway HT is the only commercially available self-balancing vehicle in the world to date. The Segway HT began its life when engineer, Dean Kamen, slipped while exiting the shower and his body threw himself backwards to try and counteract the slip. Even though he crashed to the floor, he began thinking afterwards that if the human body could respond quickly, a machine should also be able to. In 2001, the first Segway was shown on public television and was made available for purchase in 2002 [1].

The Segway control and processor system is made up of two circuit boards which sample the balance sensor assembly at 100Hz and output commands to the motors at 1000Hz with each board being responsible to one of the two motors. The Segway HT uses the Texas Instruments TMS320LF2406A Digital Signal Processor (DSP) which runs at 40 millions of instructions per second (MIPS), has 32 kilobytes (kB) of flash memory and many peripheral communication ports implemented on-board the chip. The Segway HT uses the DSPs to implement digital closed loop motor control and balance computation.

Figure 1.2: Photographs of the Segway HT i2.

### 1.2.2 The Grasser Model, 2002

Researchers at the Industrial Electronics Laboratory at the Swiss Federal Institute of Technology have built a scaled down prototype of a Digital Signal Processor controlled two-wheeled vehicle based on the inverted pendulum with weights attached to the system to simulate a human driver. A linear state space controller utilizing sensory information from a gyroscope and motor encoders are used to stabilize this system [2].

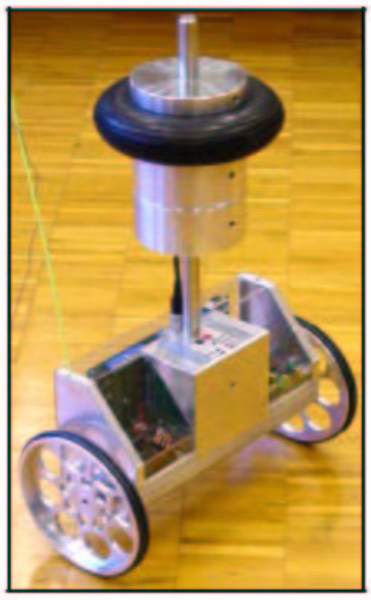

Figure 1.3: Photograph of JOE: A Mobile, Inverted Pendulum.

### 1.2.3 The Blackwell Model, 2005

This model is a successful attempt to build a self-balancing scooter similar to the Segway HT that was completed in 2002. The mechanical construction of the vehicle is simple and made from only a few off-the-shelf parts. This is advantageous as it makes the construction inexpensive and easy to both manufacturing and assembling. This model is mechanically much simpler than any other kind of vehicle. The control system of the vehicle is run from an 8-bit Atmel microcontroller using Proportional Derivative (PD) control with feedback from a piezoelectric rate gyroscope. The weakness of this setup is the need to tune by hand the proportional and derivative gains whilst actually using the vehicle. It is safer to tune the control system in a virtual simulation or with a rapid prototyping tool [3].

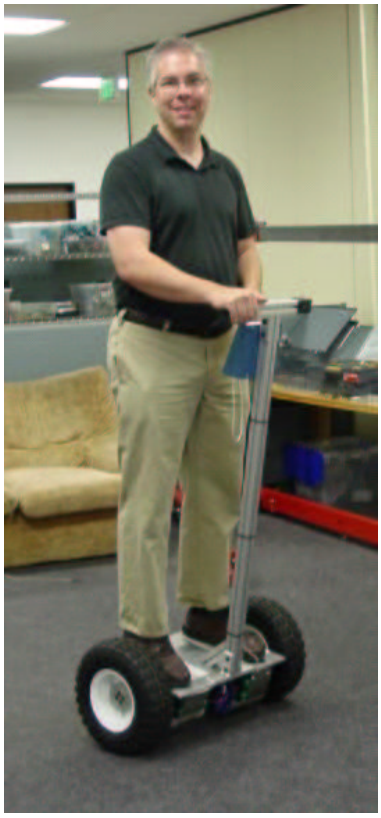

Figure 1.4: Photograph of Blackwell vehicle.

### 1.2.4 The Beckwith Model, 2004

The Human Transport Vehicle (HTV) Project aims to construct a two-wheeled balancing vehicle to explore the electronic fundamentals behind an inverted pendulum as well as solutions to modern day transportation problems. The vehicle is a two-wheeled coaxial scooter based around the Segway HT design. It uses data from a gyroscope and an accelerometer directed to a PIC microcontroller in order to balance. Modern fuzzy logic control techniques are utilized on the microcontroller to provide balance for the system [4].

Figure 1.5: Photograph of Human Transport Vehicle (HTV) project.

### 1.2.5 The Chudleigh Model, 2005

The Almost Self-Balancing 2 Wheeled Electric Skateboard [5], is a project that involves retrofitting the skateboard with two wheels and motors, and uses practical automatic control to make a skateboard balance on the two coaxial wheels positioned under the centre of the skateboard. As opposed to the Segway HT's inertial

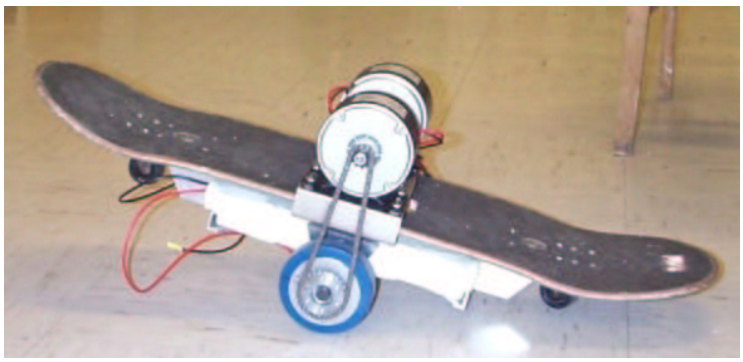

Figure 1.6: Photograph of Project Emanual skateboard.

sensors, the vehicle uses proximity sensors on the undercarriage to determine how far the end of the board is from the ground. The board is mounted on rubber bushings which enable it to roll a few degrees either side of horizontal and underneath the center of the board. On either side, there are Infra-Red (IR) sensors which enable the direction and amount of roll to be quantified for steering. The data from these sensors is fed to the PIC microcontroller for output to the motors with a percentage added or subtracted for steering.

### 1.2.6 Baloh and Parent model, 2003

This model is presented as an on-demand, fully automatic taxi service in an urban environment [6]. Like the Segway, it is principally a self balancing machine whose wheels share a common axis. However, the control objective is different since the intended use of the two vehicles are unalike the Segway longitudinal acceleration and thus velocity are controlled by the torque disturbance of the driver. Thus, when a driver leans forward, the Segway accelerates forward to prevent the passenger from falling. This is the typical response of an inverted pendulum. In contrast, the Baloh and Parent model trajectory must be entirely controlled by the steering computer. Thus, the passenger motion is a disturbance to be rejected. Furthermore, it is meant as an alternative road vehicle, not intended for sidewalk.

Figure 1.7: The Baloh and Parent model as envisioned for public service.

## 1.3 Modeling and Control

The system is basically made up of a platform that is mounted on two wheels activated independently by two DC motors. On this platform, there is a mass that can be represented as a mass point at a distance $l$ from the base plane. By looking at previous attempts of self-balancing vehicles and mobile inverted pendulums, a suitable free body diagram was found. The model chosen was based on the Grasser model [2], but with some simplification of the equations. The equation of motion for a two-wheeled inverted pendulum and linear model for a DC motor was derived. The pendulum and wheel dynamics are analyzed separately at the beginning, but this will eventually lead to two equations of motion which completely describe the behavior of the balancing problem.

Utilizing the dynamic model developed for balancing a two wheeled inverted pendulum a PD controller is designed. Since we are trying to control the pendulum's position, which should return to the vertical after the initial disturbance, the reference signal we are tracking should be zero. The force applied to the vehicle can be added as a disturbance.

## 1.4 Research Results and Contributions

This research presents a segway whose behavior is based on the stabilization of an inverted pendulum. This vehicle has been manufactured using low-cost commercial components. An experimentation system has been obtained and allows to test various controllers. The model has been tested for its balance by running a Proportional Derivative (PD) algorithm on a microprocessor chip. The model has been identified in order to serve as an educational experimental platform for segways.

## 1.5 Thesis Structure

There are six chapters in this thesis. Chapter 1 provides introduction and Literature review. Chapter 2 includes the derivation of the mathematical model of the Segway. Chapter 3 presents the design of the control system and stability analysis. Chapter 4 discusses the implementation of the system including issues of designing and selecting hardware and structural related components, detailing hardware considerations including sensors and the drive system. Chapter 5 discusses the sensors used in the design and the treatment of sensor information together with experimental results. Finally in chapter 6, conclusions and suggestions for future work are given.

# Chapter 2

# System Modeling

## 2.1 Introduction

The Segway is inherently unstable, and as such needs a control system to be able to keep it upright. This control system must take measurements of the vehicle's current state and determine what signals to apply to the motors in order to achieve a desired response. Generally a control system is designed using the following stages:

- First a mathematical model of the system is derived. This needs to be as accurate as possible whilst trading off against complexity.
- The system is then identified by analyzing the model and its response to various inputs.
- From the results of the previous step, a suitable control system can then be designed.
- The control system is then tuned to achieve a desired response using the mathematical model. Often simulation tools such as Simulink are used to help.
- Finally, when the real device is available, the tuned control system is then implemented into hardware.
- Ideally, the process would stop here, but realistically the controller would then need to be retuned with focus given on making sure that the control system is robust to changes in the device, such as extra weight and different wheels.

According to this design methodology, the first step requires a mathematical model of the Segway. The system is basically made up of a platform that is mounted on two wheels activated independently by two DC motors. On this platform, there is a mass that can be represented as a mass point at a distance $l$ from the base plane. By looking at previous attempts of self-balancing vehicles and mobile inverted pendulums, a suitable free body diagram is found. The model chosen is based on the Grasser model [2], but with some simplification of the equations. The equation of motion for a two-wheeled inverted pendulum and linear model for a DC motor is derived. The pendulum and wheel dynamics are analyzed separately at

the beginning, but this will eventually lead to two equations of motion which completely describe the behavior of the balancing problem. Three bodies are used, the two rotating masses of the wheels and the chassis/person combined body, which was represented using a single point mass at a certain distance from the axle. The latter is possible as it is anticipated that the person would be significantly heavier than the base itself. In the following sections, the equation of motion for a two-wheeled inverted pendulum and linear model for a DC motor is derived in detail.

## 2.2 Linear Model of a DC Motor

The segway is powered by two DC motors. In this section state space model of the DC motor is derived. This model is then used in the dynamic model of balancing Segway to provide a relationship between the input voltage to the motors and the control torque needed to balance the Segway.

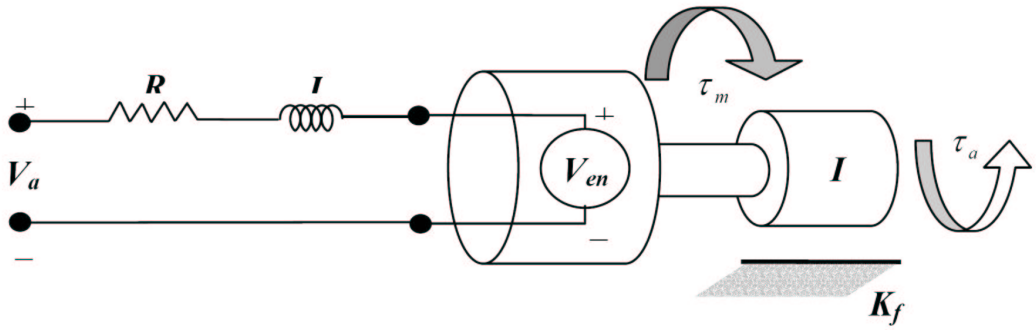


Figure 2.1: Diagram of a DC motor.

Figure 2.1 exemplifies an effective linear model for a direct current motor. When a voltage is applied to the terminals of the motor, a current $i$, is generated in the motor armature. The motor produces a torque $\tau_m$ , which is proportional to the current. This relationship can be expressed as,

$$\tau_m = k_m i \tag{2.1}$$

where: $k_m$ - is the constant of the motor torque.

The EMF voltage $V_e$ of the motor is proportional to the angular velocity of the motor spin.

$$V_e = k_e \omega \tag{2.2}$$

where:

$k_e$ - is the constant of the back EMF,
$\omega$ - is the angular velocity of the motor.

At this point, a linear differential equation for the DC motor's electrical circuit can be written by using Kirchoff's Voltage Law, the law states that the sum of all

voltages in the circuit must equal to zero. For the DC motor, this can be written as,

$$V_a - Ri - L\frac{di}{dt} - V_e = 0 \tag{2.3}$$

So

$$\frac{di}{dt} = \frac{V_a}{L} - \frac{R}{L}i - \frac{V_e}{L} \tag{2.4}$$

In deriving the equation of motion for the motor, the friction on the shaft of the motor is approximated as a linear function of the shaft velocity. The approximation that the friction on the shaft of the motor $k_f$ , is a linear function of the shaft velocity is made. Newton's law of motion states that the sum of all forces applied on the shaft is linearly related to the acceleration of the shaft multiplied by its moment of inertial $I_R$. Therefore, the preceding statement can be written as,

$$\sum M = I_R\ddot{\theta} = \tau_m - k_f\omega - \tau_a \tag{2.5}$$

So

$$\frac{d\omega}{dt} = \ddot{\theta} = \frac{\tau_m}{I_R} - \frac{k_f}{I_R}\omega - \frac{\tau_a}{I_R} \tag{2.6}$$

Substituting equation (2.1) and (2.2) into equations (2.4) and (2.6) and rearranging in terms of the time derivatives, leads to the following two fundamental equations which govern the motion of the motor.

$$\frac{di}{dt} = \frac{V_a}{L} - \frac{R}{L}i - \frac{k_e}{L}\omega \tag{2.7}$$

$$\frac{d\omega}{dt} = \frac{k_m}{I_R}i - \frac{k_f}{I_R}\omega - \frac{\tau_a}{I_R} \tag{2.8}$$

Both equations are linear functions of current and velocity and they include the first order time derivatives. A simplified DC motor model is sufficient for the balancing case. For that reason, the motor inductance and motor friction is considered negligible and is approximated as zero. Hence, equations (2.7)and (2.8) can be approximated as,

$$i = \frac{V_a}{R} - \frac{k_e}{R}\omega \tag{2.9}$$

$$\frac{dw}{dt} = \frac{k_m}{I_R}i - \frac{\tau_a}{I_R} \tag{2.10}$$

By substituting equation (2.9) into equation (2.10), an approximation for the DC motor which is only a function of the current motor speed, applied voltage and applied torque are obtainable.

$$\frac{dw}{dt} = \frac{k_m}{I_R R}V_a - \frac{k_m k_e}{I_R R}\omega - \frac{\tau_a}{I_R} \tag{2.11}$$

The motor's dynamic model can be represented with a state space expression.

$$\begin{bmatrix} \dot{\theta} \\ \dot{\omega} \end{bmatrix} = \begin{bmatrix} 0 & 1 \\ 0 & -\frac{k_m k_e}{I_R R} \end{bmatrix} \begin{bmatrix} \theta \\ \omega \end{bmatrix} + \begin{bmatrix} 0 & 0 \\ \frac{k_m}{I_R R} & -\frac{1}{I_R} \end{bmatrix} \begin{bmatrix} V_a \\ \tau_a \end{bmatrix} \tag{2.12}$$

$$[y] = \begin{bmatrix} 1 & 0 \end{bmatrix} \begin{bmatrix} \theta \\ \omega \end{bmatrix} + \begin{bmatrix} 0 & 0 \end{bmatrix} \begin{bmatrix} V_a \\ \tau_a \end{bmatrix}$$

where:

$\theta$ - is the angular position,
$\omega$ - is the angular velocity.
$\tau_a$ - is the applied torque.

Applied voltage and applied torque of the DC motor are inputs of this model. This is a first order differential equation.

## 2.3 Dynamic Model for a Two Wheeled Inverted Pendulum

The two-wheeled inverted pendulum, albeit more complex in system dynamics, has similar behavior with a pendulum on a cart. The pendulum and wheel dynamics are analyzed separately at the beginning, but this will eventually lead to two equations of motion which completely describe the behavior of the balancing Segway. Three bodies were used, the two rotating masses of the wheels and the chassis/person combined body, which was represented using a single point mass at a certain distance from the axle. The latter was possible as it was anticipated that the person would be significantly heavier than the base itself.

Firstly the equations of motion associated with the left and right wheels are obtained. Figure 2.2 shows the free body diagram for both wheels. Since the equation for the left and right wheels are completely analogous, only the equation for the right wheel is given.

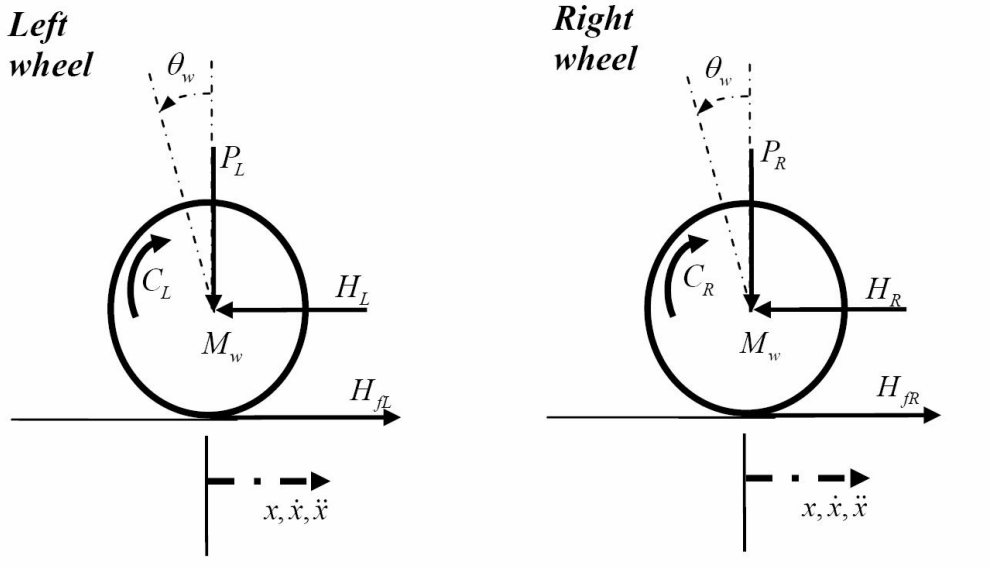


Figure 2.2: Free body diagram of the wheels.

Using Newton's law of motion, the sum of forces on the horizontal $x$ direction is

$$\sum F_x = M_w a = M_w \ddot{x} = H_{fR} - H_R \tag{2.13}$$

where:

$M_w$ - is the mass of the wheel,
$H_{fR}$ - is the horizontal friction,
$H_R$ - is the horizontal force.

Sum of moments of forces around the center of the wheel gives,

$$\sum M_o = I_w a = I_w \ddot{\theta_w} = C_R - H_{fR} r \tag{2.14}$$

where:

$I_w$ - is the inertia of the wheel,
$r$ - is the radius of the wheel,
$C_R$ - is the output torque to the wheels

From DC motor dynamics, the motor torque can be expressed as,

$$\tau_m = I_R \frac{d\omega}{dt} + \tau_a \tag{2.15}$$

Rearranging the equation and substituting the parameters from the DC motor derivation section, the output torque to the wheels is attained.

$$C_R = I_R \frac{d\omega}{dt} + \tau_a = \frac{-k_m k_e}{R} \dot{\theta_w} + \frac{k_m}{R} V_a \tag{2.16}$$

Therefore, equation (2.14) becomes,

$$I_w \ddot{\theta_w} = \frac{-k_m k_e}{R} \dot{\theta_w} + \frac{k_m}{R} V_a - H_{fR} r \tag{2.17}$$

Thus,

$$H_{fR} = \frac{-k_m k_e}{Rr} \dot{\theta_w} + \frac{k_m}{Rr} V_a - \frac{I_w \ddot{\theta_w}}{r} \tag{2.18}$$

Equation (2.18) is substituted into (2.13) to get the equation for the left and right wheels. For the left wheel,

$$M_w \ddot{x} = \frac{-k_m k_e}{Rr} \dot{\theta_w} + \frac{k_m}{Rr} V_a - \frac{I_w \ddot{\theta_w}}{r} - H_L \tag{2.19}$$

For the right wheel,

$$M_w \ddot{x} = \frac{-k_m k_e}{Rr} \dot{\theta_w} + \frac{k_m}{Rr} V_a - \frac{I_w \ddot{\theta_w}}{r} - H_R \tag{2.20}$$

Because the linear motion is acting on the centre of the wheel, the angular rotation can be transformed into linear motion by simple transformation,

$$\ddot{\theta_w} r = \ddot{x} \Rightarrow \ddot{\theta_w} = \frac{\ddot{x}}{r}$$

$$\dot{\theta_w} r = \dot{x} \Rightarrow \dot{\theta_w} = \frac{\dot{x}}{r}$$

By the linear transformation, equation (5.19) and (5.20) becomes:

For the left wheel,

$$M_w \ddot{x} = \frac{-k_m k_e}{Rr^2}\dot{x} + \frac{k_m}{Rr}V_a - \frac{I_w \ddot{x}}{r^2} - H_L \tag{2.21}$$

For the right wheel,

$$M_w \ddot{x} = \frac{-k_m k_e}{Rr^2}\dot{x} + \frac{k_m}{Rr}V_a - \frac{I_w \ddot{x}}{r^2} - H_R \tag{2.22}$$

Adding equation (2.21) and (2.22) together yields,

$$2(M_w + \frac{I_w}{r^2})\ddot{x} = \frac{-2k_m k_e}{Rr^2}\dot{x} + \frac{2k_m}{Rr}V_a - (H_R + H_R) \tag{2.23}$$

The vehicle's chassis can be modeled as an inverted pendulum. Figure 2.3 shows the free body diagram of the chassis.

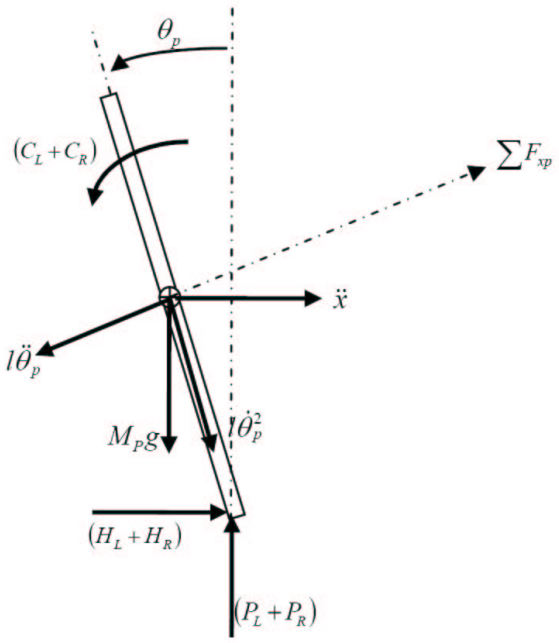


Figure 2.3: Free body diagram of the chassis.

Again, by using Newton's law of motion, the sum of forces in the horizontal direction is as follows.

$$\sum F_x = M_p\ddot{x} = (H_L + H_R) - M_p l\ddot{\theta}_p \cos\theta_p + M_p l\dot{\theta_p}^2 \sin\theta_p \tag{2.24}$$

thus,

$$(H_L + H_R) = M_p\ddot{x} + M_p l\ddot{\theta}_p \cos\theta_p - M_p l\dot{\theta_p}^2 \sin\theta_p \tag{2.25}$$

Where :

$M_p$ - is the mass of the vehicle and the rider system,
$l$ - is the length of the pendulum center of mass,
$\theta$ - is the angle of the chassis and the horizontal line.

The sum of forces perpendicular to the pendulum,

$$\sum F_{xp} = M_p\ddot{x}\cos\theta_p = (H_L + H_R)\cos\theta_p + (P_L + P_R)\sin\theta_p - M_p g\sin\theta_p - M_p l\ddot{\theta}_p \tag{2.26}$$

The sum of moments around the centre of mass of pendulum,

$$\sum M_o = I\alpha = I_p\ddot{\theta}_p = -(H_L + H_R)l\cos\theta_p - (P_L + P_R)l\sin\theta_p - (C_L + C_R) \tag{2.27}$$

$I_p$ - is the inertia of the system (vehicle + rider),
$P_L, P_R$ - are reaction forces between wheels and chassis,

The torque applied on the pendulum from the motor as defined in equation (2.16) and after linear transformation,

$$C_L + C_R = 2C = \frac{-2k_m k_e}{Rr}\dot{x} + \frac{2k_m}{R}V_a \tag{2.28}$$

Substituting this into equation (2.27) gives,

$$I_p\ddot{\theta_p} = -(H_L + H_R)l\cos\theta_p - (P_L + P_R)l\sin\theta_p - (\frac{-2k_m k_e}{Rr}\dot{x} + \frac{2k_m}{R}V_a) \tag{2.29}$$

thus,

$$I_p\ddot{\theta}_p - \frac{2k_m k_e}{Rr}\dot{x} + \frac{2k_m}{R}V_a = -(H_L + H_R)l\cos\theta_p - (P_L + P_R)l\sin\theta_p \tag{2.30}$$

Multiply equation (2.26) by $-l$,

$$-M_p\ddot{x}\cos\theta_p l = [-(H_L+H_R)l\cos\theta_p - (P_L+P_R)l\sin\theta_p] + M_p gl\sin\theta_p + M_p l^2\ddot{\theta}_p \tag{2.31}$$

Substitute equation (2.30) in equation (2.31),

$$I_p\ddot{\theta}_p - \frac{2k_m k_e}{Rr}\dot{x} + \frac{2k_m}{R}V_a = -M_p\ddot{x}\cos\theta_p l - M_p gl\sin\theta_p - M_p l^2\ddot{\theta}_p \tag{2.32}$$

Substituting equation (2.25) into (2.23) eliminates $(H_L + H_R)$,

$$2(M_w + \frac{I_w}{r^2})\ddot{x} = -\frac{2k_m k_e}{Rr^2}\dot{x} + \frac{2k_m}{Rr}V_a - M_p\ddot{x} - M_p l\ddot{\theta_p}cos\theta_p + M_p l\dot{\theta_p^2}sin\theta_p \quad (2.33)$$

Rearranging equations (3.32) and (3.33) gives the non-linear equations of motion of the system,

$$(I_p + M_p l^2)\ddot{\theta_p} - \frac{2k_m k_e}{Rr}\dot{x} + \frac{2k_m}{R}V_a + M_p gl sin\theta_p = -M_p\ddot{x}cos\theta_p \quad (2.34)$$

$$(2M_w + M_p + \frac{2I_w}{r^2})\ddot{x} + \frac{2k_m k_e}{Rr}\dot{x} + M_p l\ddot{\theta_p}cos\theta_p - M_p l\dot{\theta_p^2}sin\theta_p = \frac{2k_m}{R}V_a \quad (2.35)$$

Assuming that $\theta_p = \pi + \varphi$, where $\varphi$ represents a small angle from vertical upright direction, these two equations can be linearized.

$$cos\theta_p = -1, \qquad sin\theta_p = -\varphi, \qquad (\frac{d\theta_p}{dt})^2 = 0.$$

The linearized equations of motion is,

$$(I_p + M_p l^2)\ddot{\varphi_p} - \frac{2k_m k_e}{Rr}\dot{x} + \frac{2k_m}{R}V_a - M_p gl\varphi_p = M_p l\ddot{x} \quad (2.36)$$

$$(2M_w + M_p + \frac{2I_w}{r^2})\ddot{x} + \frac{2k_m k_e}{Rr^2}\dot{x} - M_p l\ddot{\varphi_p} = \frac{2k_m}{Rr}V_a \quad (2.37)$$

### 2.3.1 State Space Representation of the System

Rearrange equation (3.36) and (3.37)to get the state space representation of the system,

$$\ddot{\varphi} = \frac{M_p l}{I_p + M_p l^2}\ddot{x} + \frac{2k_m k_e}{(I_p + M_p l^2)Rr}\dot{x} - \frac{2k_m}{(I_p + M_p l^2)R}V_a + \frac{M_p gl}{(I_p + M_p l^2)}\varphi \quad (2.38)$$

$$\ddot{x} = \frac{2k_m}{(2M_w + M_p + \frac{2I_w}{r^2})Rr}V_a - \frac{2k_m k_e}{(2M_w + M_p + \frac{2I_w}{r^2})Rr^2}\dot{x} + \frac{M_p l}{(2M_w + M_p + \frac{2I_w}{r^2})}\ddot{\varphi} \quad (2.39)$$

By substituting equation (5.38) into equation (5.36), substituting equation (5.39) into equation (5.37) and after a series of algebraic manipulation the state space equation for the system is obtained.

$$\begin{bmatrix} \dot{x} \\ \ddot{x} \\ \dot{\varphi} \\ \ddot{\varphi} \end{bmatrix} = \begin{bmatrix} 0 & 1 & 0 & 0 \\ 0 & \frac{2K_m K_e(M_p lr - Ip - M_p l^2)}{Rr^2\alpha} & \frac{M_p^2 gl^2}{\alpha} & 0 \\ 0 & 0 & 0 & 1 \\ 0 & \frac{2K_m K_e(r\beta - M_p l)}{Rr^2\alpha} & \frac{M_p gl\beta}{\alpha} & 0 \end{bmatrix} \begin{bmatrix} x \\ \dot{x} \\ \varphi \\ \dot{\varphi} \end{bmatrix} + \begin{bmatrix} 0 \\ \frac{2K_m(I_p + M_p l^2 - M_p lr)}{Rr^2\alpha} \\ 0 \\ \frac{2K_m(M_p l - r\beta)}{Rr\alpha} \end{bmatrix} V_a. \quad (2.40)$$

Where:

$$\alpha = I_p\beta + 2M_p l^2(M_w\frac{I_w}{r^2}),$$

$$\beta = 2M_w + \frac{2I_w}{r^2} + M_p.$$

This model of the system assumes that the wheels of the vehicle will always stay in contact with ground and there is no slip at the wheels.

### 2.3.2 System Parameters

The definitions of parameters are shown in Table 2.1 and Table 2.2. All parameters are calculated and measured based on Appendix A.

Table 2.1: Definitions of variable parameters of the system.

| Parameter | Definition | Value |
|---|---|---|
| $x$ | Distance | m |
| $\dot{x}$ | Speed | m/s |
| $\ddot{x}$ | Acceleration | $m/s^2$ |
| $\varphi$ | Error angle | rad |
| $\dot{\varphi}$ | Error angular speed | rad/s |
| $\ddot{\varphi}$ | Error angular acceleration | $rad/s^2$ |

Table 2.2: Definitions of constant parameters of the system.

| Parameter | Definition | Value |
|---|---|---|
| $k_m$ | Constant of the motor torque | 0.864 Nm/A |
| $k_e$ | Constant of the motor's back-EMF | 0.097 Vs/rad |
| $l$ | Length of the pendulum | 1.7 m |
| $r$ | Wheel radius | 0.2 m |
| $R$ | Resistance of the Motor | 1Ω |
| $M_p$ | Mass of the pendulum | 85 kg |
| $I_p$ | Moment of inertia of the pendulum | 68.07 kg.m$^2$ |
| $M_w$ | Mass of the wheel | 3.5 kg |
| $I_w$ | Inertia of the wheel | 0.07 kg.m$^2$ |
| $g$ | Acceleration of gravity | 9.8 m/s$^2$ |

Based on the this parameter values the state space equation and the transfer function for the system is obtained as

$$\begin{bmatrix} \dot{x} \\ \ddot{x} \\ \dot{\varphi} \\ \ddot{\varphi} \end{bmatrix} = \begin{bmatrix} 0 & 1 & 0 & 0 \\ 0 & -0.0645 & 6.4143 & 0 \\ 0 & 0 & 0 & 1 \\ 0 & -0.0290 & 9.0084 & 0 \end{bmatrix} \begin{bmatrix} x \\ \dot{x} \\ \varphi \\ \dot{\varphi} \end{bmatrix} + \begin{bmatrix} 0 \\ 0.0.1330 \\ 0 \\ 0.0597 \end{bmatrix} V_a \tag{2.41}$$

$G(s) = G_1(s) + G_2(s)$

$$G_2(s) = \frac{X(s)}{V_a(s)} = \frac{0.1330s^2 - 0.8150}{s^4 + 0.0645s^3 - 9.0084s^2 - 0.3953s} \tag{2.42}$$

$$G_1(s) = \frac{\varphi(s)}{V_a(s)} = \frac{0.0597s^2}{s^4 + 0.0645s^3 - 9.0084s^2 - 0.3953s} \tag{2.43}$$

The schematic block diagram for this open loop system is shown in Figure 2.4.

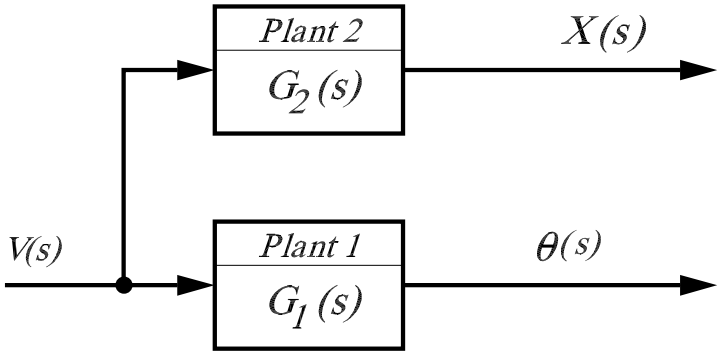


Figure 2.4: Schematic block diagram for the open loop system.

# Chapter 3

# Control System Design

The balancing system described in chapter 2 is an excellent test bed for control theory because it exhibits non-linear and unstable system dynamics. Control objectives for these systems are always challenging. Therefore, in this chapter, it is our aim to show how the system can be controlled using PID controllers. The controllers are designed utilising the dynamics model developed in the previous chapter.

We will implement a PD controller which can only be applied to a single-input-single-output (SISO) system, so we will be only interested in the control of the pendulums angle. Therefore, none of the design criteria deal with the vehicle position. The control of this problem is a little different than the standard control problems we are used to. Since we are trying to control the pendulum's position, which should return to the vertical after the initial disturbance, the reference signal we are tracking should be zero. The schematic for this problem should look like the diagram shown in Figure 3.1.

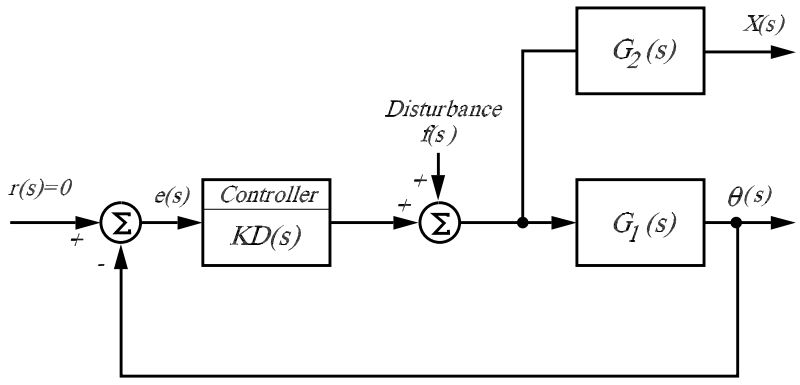


Figure 3.1: Schematic block diagram for the closed loop system.

Where,

$$G_2(s) = \frac{X(s)}{V_a(s)} = \frac{0.1330s^2 - 0.8150}{s^4 + 0.0645s^3 - 9.0084s^2 - 0.3953s}$$

$$G_1(s) = \frac{\varphi(s)}{V_a(s)} = \frac{0.0597s^2}{s^4 + 0.0645s^3 - 9.0084s^2 - 0.3953s}$$

and D(s) is the transfer function of the PID controller equals

$$D(s) = K_c \frac{K_d s^2 + K_p s + K_i}{s}$$

## 3.1 The Characteristics of P, I, and D Controllers

In the transfer function of a PID controller, the proportional control $K_p$ will have the effect of reducing the rise time and will reduce but never eliminate the steady-state error. The integral control $K_i$ will have the effect of eliminating the steady-state error, but it may make the transient response worse. The derivative control $K_d$ will have the effect of increasing the stability of the system, reducing the overshoot, and improving the transient response [7]. Effects of each of controllers $K_p$, $K_d$, and $K_i$ on a closed-loop system are summarized in Table 3.1.

Table 3.1: The effect of parts of the PID controller on the overall system response.

| Closed Loop Response | Rise Time | Overshoot | Settling Time | Steady State Error |
|---|---|---|---|---|
| $K_p$ | Decrease | Increase | Small Change | Decrease |
| $K_i$ | Decrease | Increase | Increase | Eliminate |
| $K_d$ | Small Change | Decrease | Decrease | Small Change |

Note that these correlations may not be exactly accurate, because $K_p$, $K_i$, and $K_d$ are dependent on each other. In fact, changing one of these variables can change the effect of the other two. For this reason, the table should only be used as a reference when you are determining the values for $K_i$, $K_p$ and $K_d$.

## 3.2 Analysis of Uncompensated System

The poles of the open loop linearized model of segway are 0, 2.9912, -3.0119 and -0.0439. The position of the poles shows that system is unstable, as one of the poles of the transfer function lies on the Right Half Side of the s-plane. Thus, the system is absolutely unstable. In this section the simulation results when an impulse and step inputs are applied to the uncontrolled system are presented.

### 3.2.1 Impulse Response of Open Loop System

An impulse response of the system is shown in Figure 3.2. The system is highly unstable as Theta diverges very rapidly. The runaway nature of the response indicates instability.

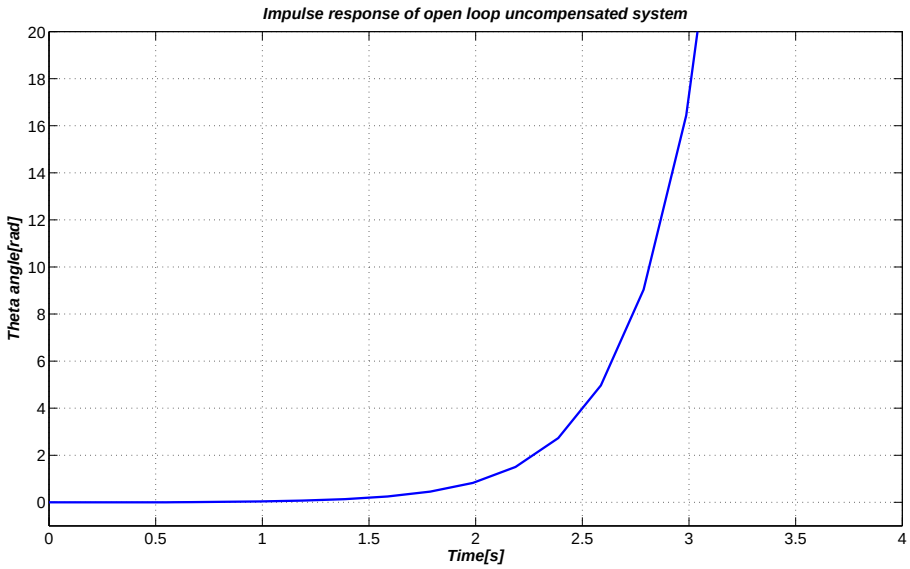


Figure 3.2: Open loop impulse response of the uncompensated system

### 3.2.2 Step Response of Open Loop System

A step response of the system is shown in Figure 3.3. Here also, Theta diverges very rapidly as the system is highly unstable. The runaway nature of the response indicates instability.

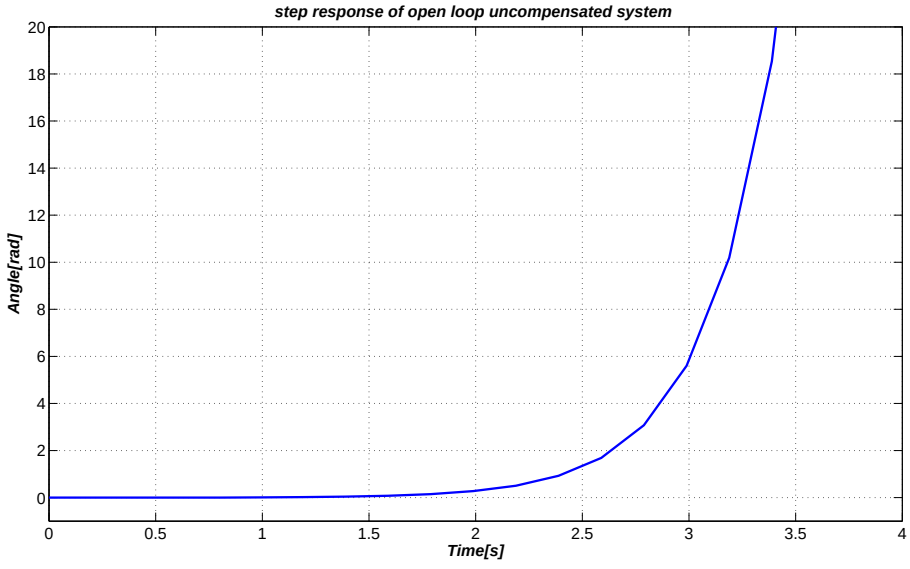


Figure 3.3: Open loop step response of the uncompensated system

### 3.2.3 Root Locus of the Uncompensated System

The first step in designing compensation for any plant is to observe the closed loop unity feedback response to check for stability. Many systems are unstable in open

loop but stable in closed loop configuration. The other way round is also possible that the system is stable in the open loop but unstable in closed loop, although this case is rare. The closed loop uncompensated system can be studied by viewing the root locus plot of the system. Figure 3.4 shows the root locus plot of the system. The plot reveals that the system cannot be controlled by a simple unity feedback loop. Whatever be the value of loop gain, $K$, one branch of the locus remains on RHS (in unstable region) of s-plane. This makes control impossible by unity feedback. The root locus has a branch on the right hand side of the imaginary axis, which indicates that *the system is unstable in closed loop for all values of* $K$. From the above analysis, it is concluded that using only the gain compensation in closed loop cannot control the system. Reshaping of the system roots is necessary so that for certain range of gains the system has all its roots in the left half plane (stable region) of the s-plane.

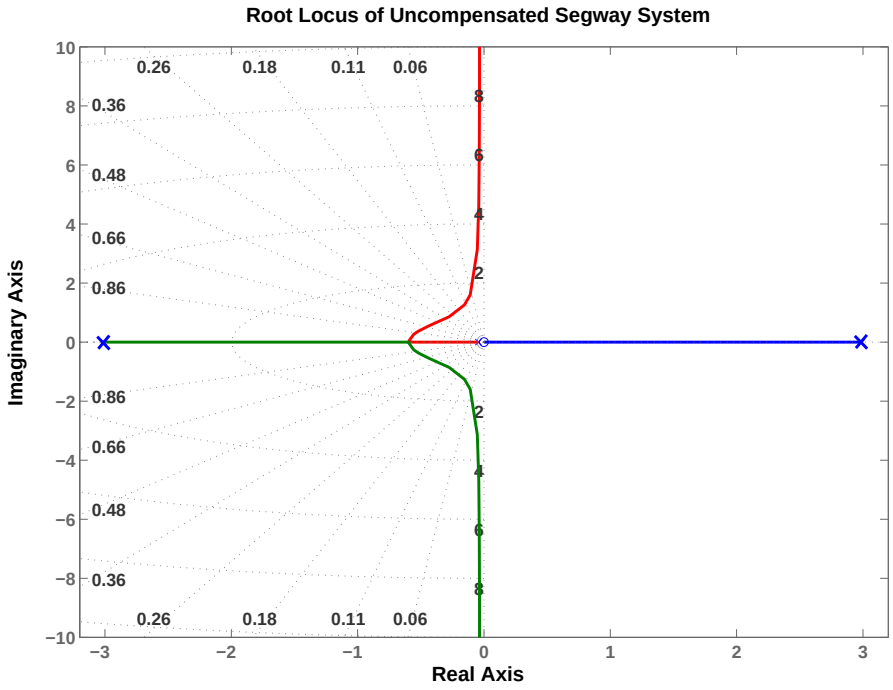


Figure 3.4: Root locus plot of the system

## 3.3 Compensation Design

The desired transient response for the system has the following characteristics:

- Transient (settling) time of 0.5 second.
- Overshoot should be $< 16\%$ (damping ratio $\zeta > 0.5$).

The desired STEADY-STATE response for the system has following characteristics:

- Steady-state error must be $< 2\%$.

### 3.3.1 Compensation Design

To implement this control problem MATLAB Simulink is used. The Simulink model of linearised model of Segway system is shown in Figure 3.5.

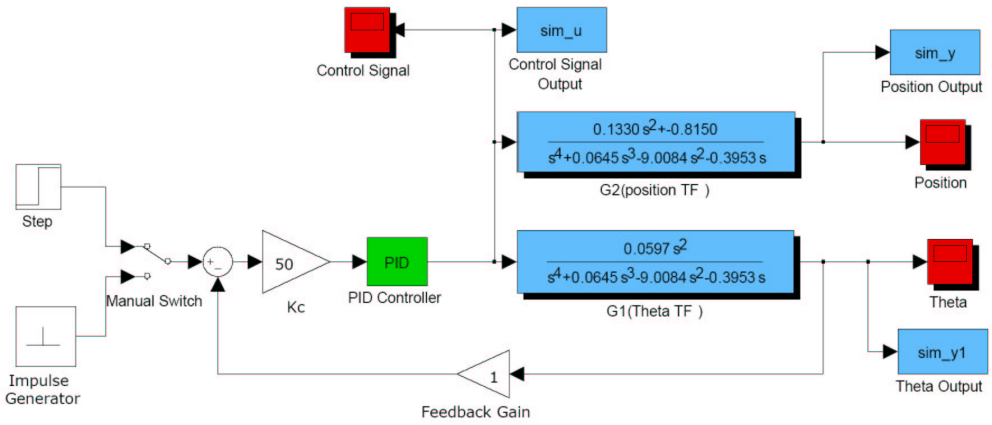


Figure 3.5: Simulink model of linearized model of control system

In this design the steps shown below are followed to obtain a desired response.

- Open-loop response is obtained and what needs to be improved is determined.
- A proportional control is added to improve the rise time.
- A derivative control is added to improve the overshoot
- An integral control is added to eliminate the steady-state error
- Each of $K_p$, $K_i$, and $K_d$ are adjusted until a desired overall response is obtained.

Finally one must keep in mind that implementing all three controllers (proportional, derivative, and integral) into a single system is not necessary. For example, if a PI controller gives a good enough response, then implementing a derivative controller on the system is not needed.
After simulating this compensated system in SIMULINK and following the previous steps the gains of the controller are found as Kc = 50, Kp = 200, Ki = 0, Kd =20.

## 3.4 Analysis of Compensated System

In this section the controlled system is analyzed. Simulation results when an impulse and step inputs are applied to the system are presented.

### 3.4.1 Root Locus of the Compensated System

As can be seen in the root locus of the compensated system shown in Figure 3.6, a PD controller can stabilize the loop. The controller have provide finite terminus

points to the two branches of the locus on LHS of the s-plane which would be, otherwise, approaching to infinity. The system is stable since all the roots are on the left-hand-side of the imaginary axis.

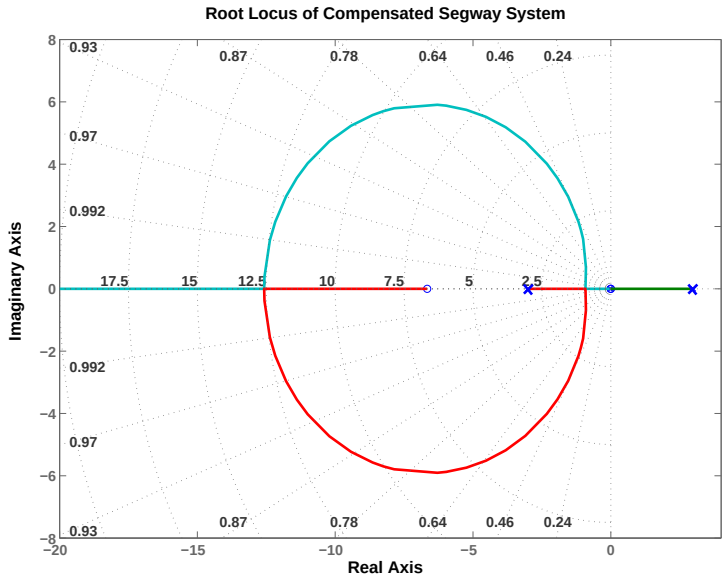


Figure 3.6: Root locus plot of the compensated system

### 3.4.2 Impulse Response of Closed Loop Comp. System

An impulse response of the PD compensated system is shown in following Figure 3.7. The response of the system is very fast, and the settling time is very small (less than 0.5 s).

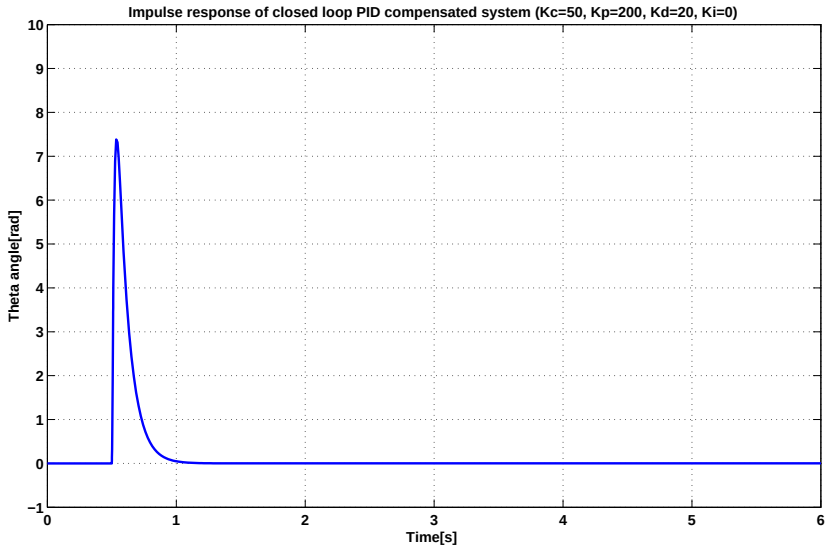


Figure 3.7: Impulse response of closed loop PD compensated system

### 3.4.3 Step Response of Closed Loop Compensated System

The step response of the PD compensated system is shown in Figure 3.8. The DC Gain of the Closed-Loop Compensated Inverted Pendulum System is 1. There is not overshoot, and the steady-state error is less than 2%.

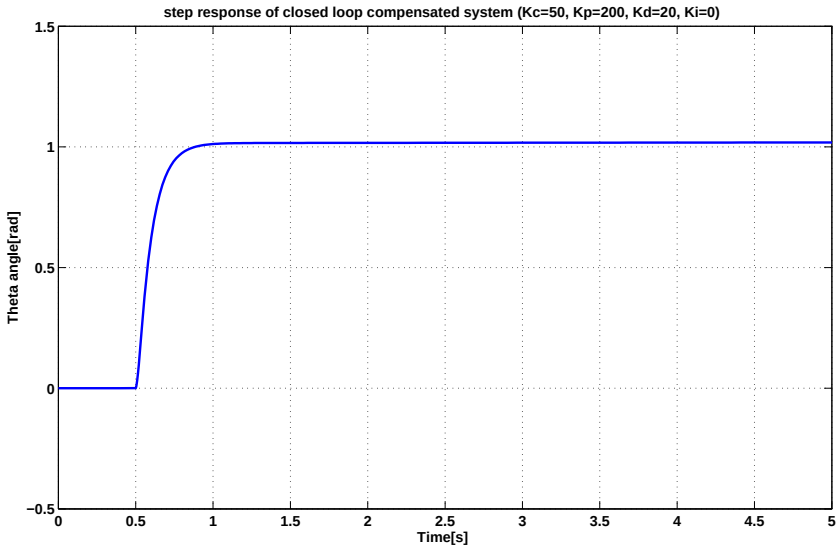


Figure 3.8: Step response of closed loop PD compensated system

### 3.4.4 Response to Disturbance in Force on the Vehicle of Closed Loop PD Compensated System

Figure 3.9 shows the Simulink model of compensated system with disturbance in the force on the vehicle.

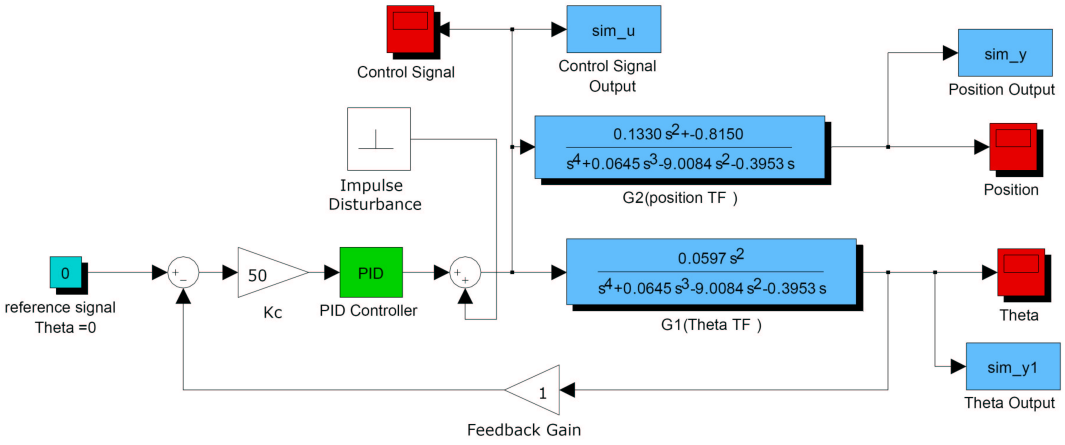


Figure 3.9: Simulink model of linearized model of the system with disturbance in force on the vehicle

The response of the closed loop compensated system to disturbance in force on the vehicle is shown in Figure 3.10. From the Figure it can be seen that the system has rejected the disturbance.

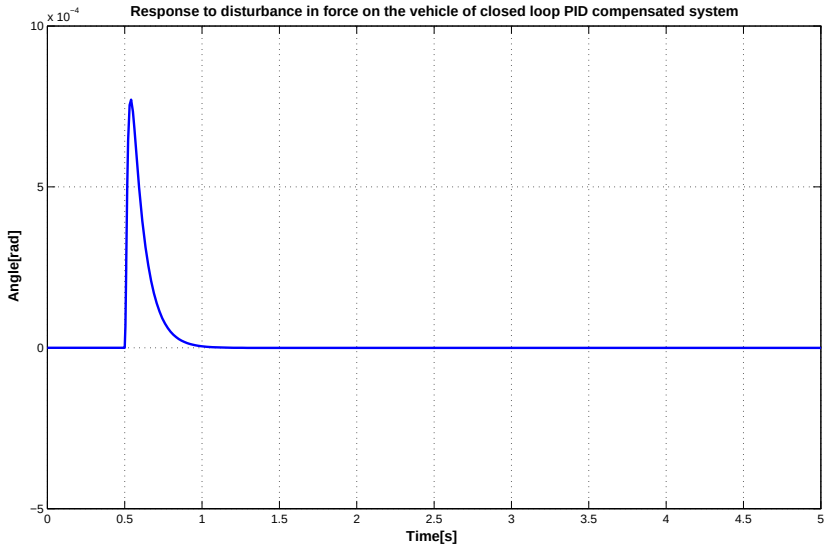


Figure 3.10: Response to disturbance in force on the vehicle of closed loop PD compensated system

### 3.4.5 Response to Disturbance in Position of the Pendulum of the Compensated System

Figure 3.11 shows the Simulink model of compensated system with disturbance in position of the pendulum.

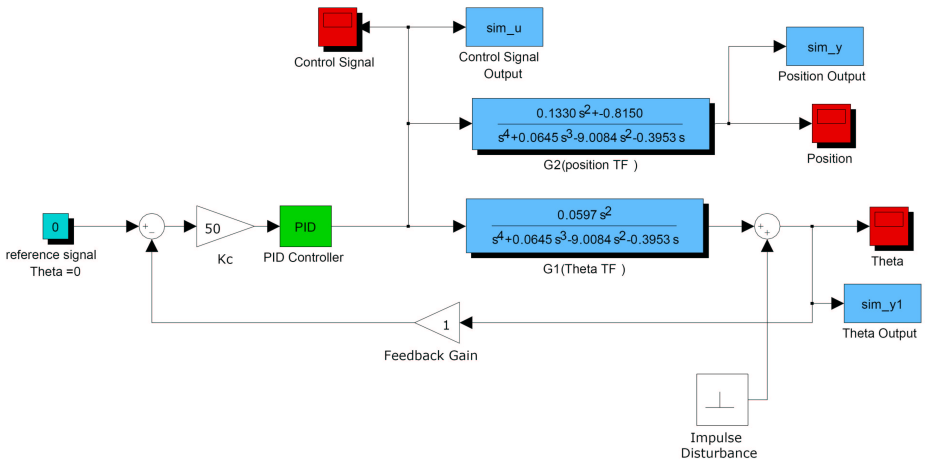


Figure 3.11: Simulink model of linearized model of the system with disturbance in position of the pendulum

The response of the closed loop compensated system to disturbance in position of the pendulum is shown in Figure 3.12. From the Figure it can be seen that the system has rejected the disturbance.

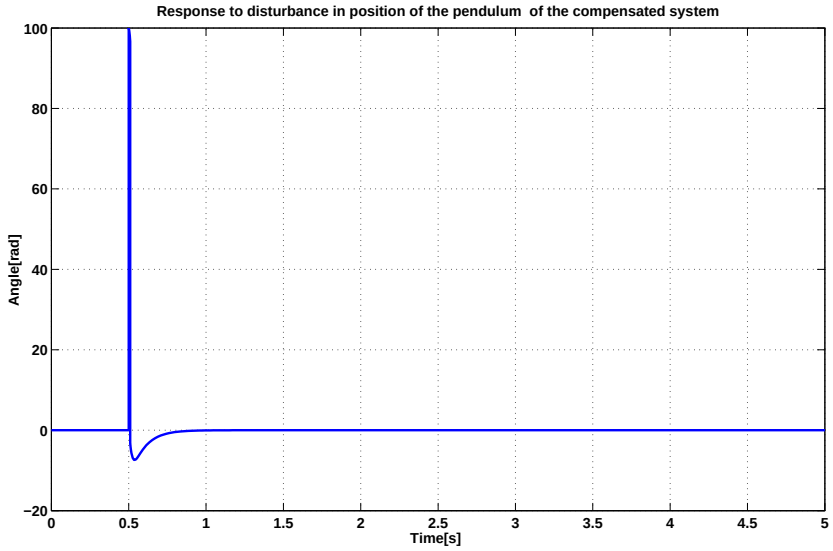


Figure 3.12: Response to disturbance in position of the pendulum of the compensated system

# Chapter 4

# Implementation

This chapter discusses the issues of designing and selecting hardware and structural related components. The selection of the components was completed gradually to meet the demands taking into account budget constraints and manufacturing complexity. The lack of existing mechanical or electrical components made quite selecting multiple components that depended on each other to satisfy specifications challenging.

## 4.1 System Architecture

The system has a low-cost microcontroller (PIC16F877A, by Microchip) [8], which communicates with various peripherals. As it can be seen in Figure 4.1, there are two sets of devices connected to the microcontroller: sensors and actuators. The set of sensors is made up by a gyroscope and an accelerometer for balancing, and a potentiometer for steering measurements. The gyroscope and accelerometer were chosen from the Analog Devices iMEMS (ADXL203EB and ADXL203EB) [9, 10]. They report an analog voltage between 0V and 5V to the controller. The gyroscope is used simply to measure angular rate. The accelerometer is used to indirectly measure the direction of the force of gravity, since it is really sensing force per unit mass along a given axis. This, along with a small angle approximation, gives an estimate of the angle to horizontal. The system actuators are two geared electric motors that run on 24VDC and are able to reach 81 rpm [11] .

Motor drivers are required to turn the control signal from the microcontroller into an appropriate varying power level to drive the motors. Figure 4.2 shows the view of the physical components from the perspective of underneath the board.

Pulse Width Modulation (PWM) is one method of communicating between a microcontroller and a motor driver [12]. By sending a train of pulses at regular intervals and varying the width of the pulses, the motor driver is able to interpret this pulse width as a requested motor duty level. Two H-bridge FET motor drivers were designed to drive the motors. The communication with the microcontroller is through a standard RS-232. This link allows to have a connection between the microcontroller and the monitoring PC. All of the code on-board the segway was written in C and compiled using mikroC, mikroElektronika C compiler for

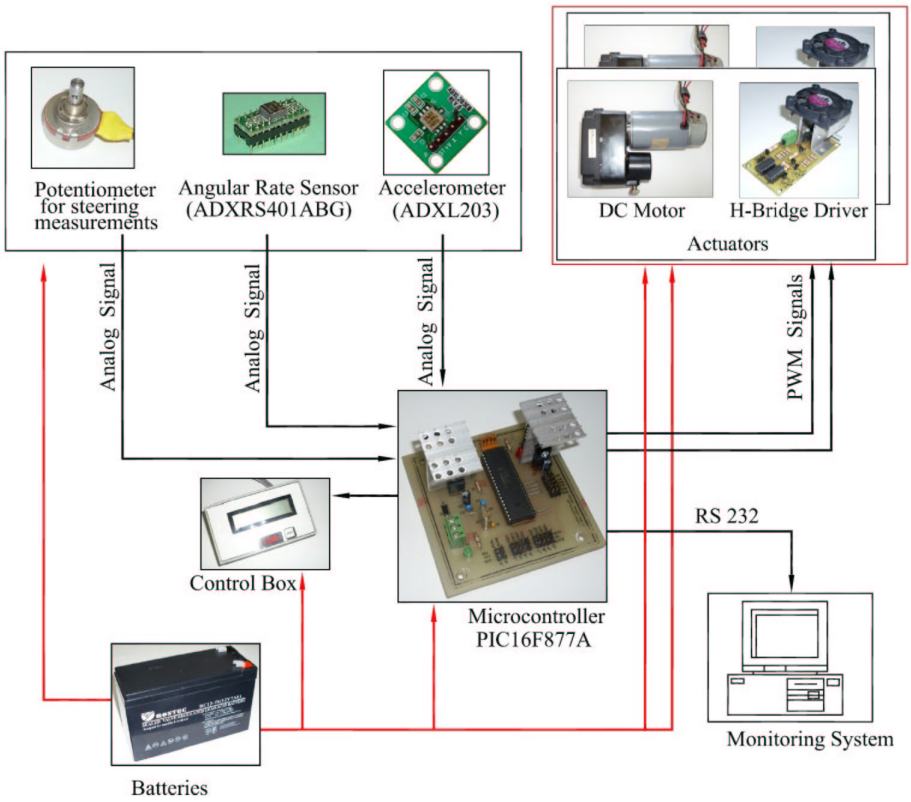


Figure 4.1: Architecture of the system.

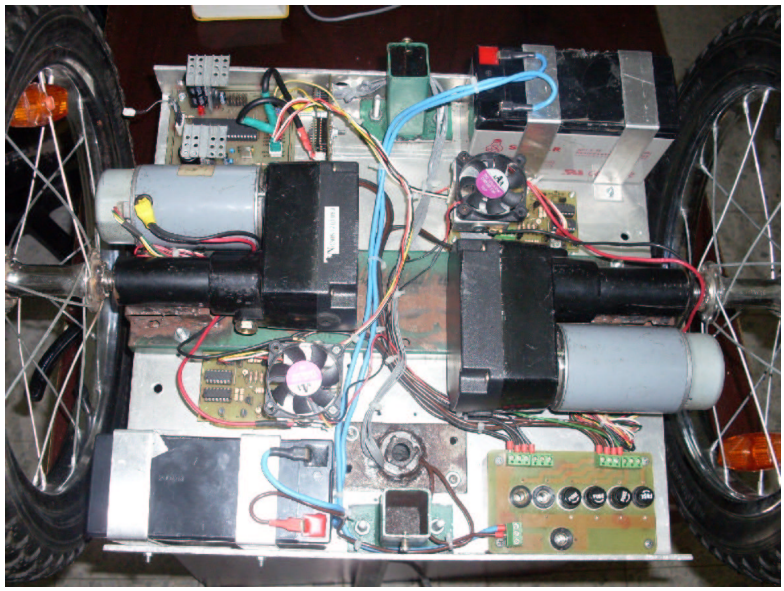

Figure 4.2: The view of the physical components from the perspective of underneath the board.

Microchip PIC microcontrollers. The code's main loop runs at about one hundred times per second (100 Hz), which is more than adequate for keeping a person balanced [13]. To carry out useful experiments, it is necessary to have a reliable way to monitor and store the data generated. This is the reason behind the development of a PC software application, with the aim of: monitoring the system variables in real time and storing the samples obtained in the experiment for subsequent study. This PC software application was implemented using Dot Net as shown in Figure 4.3.

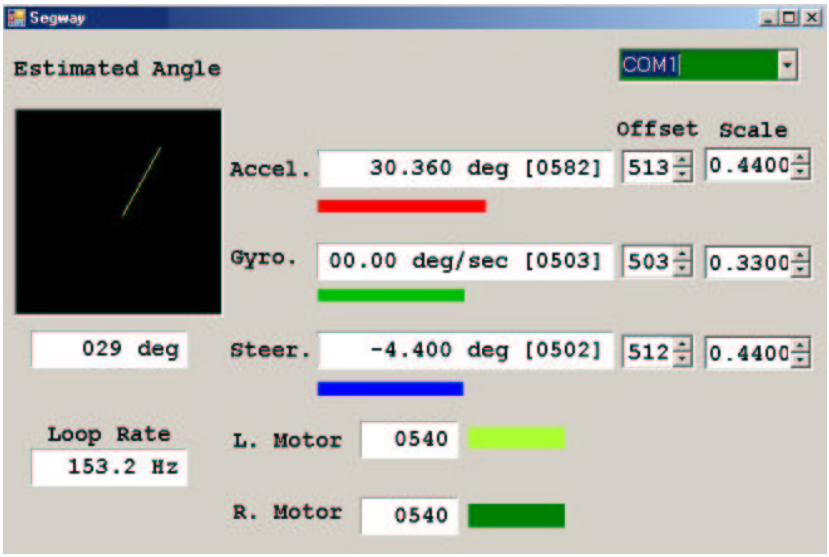


Figure 4.3: View of the implemented visual basic application.

## 4.2 Hardware Implementation

In this section the hardware and structural related component selection is discussed in detail.

### 4.2.1 Motors and Gearboxes

The actuation to balance the vehicle is via integrated DC electric motors. Two 55W electric motors form Htachi DC Motors type D06D402E are chosen to drive the segway, shown in Figure 4.4. The specifications of the motors are listed below:

- 38VDC operation
- current: 2A
- Power: 55W
- Rated speed: 3570 RPM
- Measures: 61mm Diameter x 117mm Length (+ output shaft)

- Torque: 0.06 Nm
- Torque constant: 0.0298 Nm/A
- Weight: 1.2kg

Figure 4.4: Photograph of the chosen DC motor and gear box.

A gear box of satellite dish motors with three-stage transmission and a compact 29:1 gear ratio for maximum torque transmission efficiency were chosen as shown in Figure 4.5. It uses a helical gear assembly that significantly reduces noise. The gears are also have non-integer gear ratios, so the gear teeth mesh at different points from revolution to revolution which minimizes wear on the teeth. Figure 4.6 shows the geared motor coupled to the wheels.

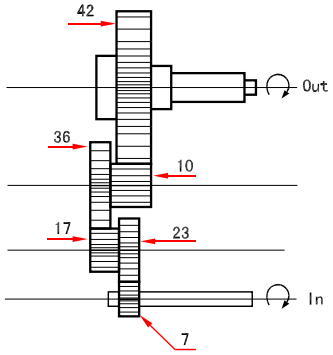


Figure 4.5: Diagram explaining the stage transmission of the gear box.

$$Gear\ Ratio = \frac{7}{23} \times \frac{17}{36} \times \frac{10}{42} = \frac{1}{29}$$

$$\frac{10}{42} = 0.3448275862$$

$$\frac{17}{36} = 0.4722222222$$

$$\frac{7}{23} = 0.2380952381$$

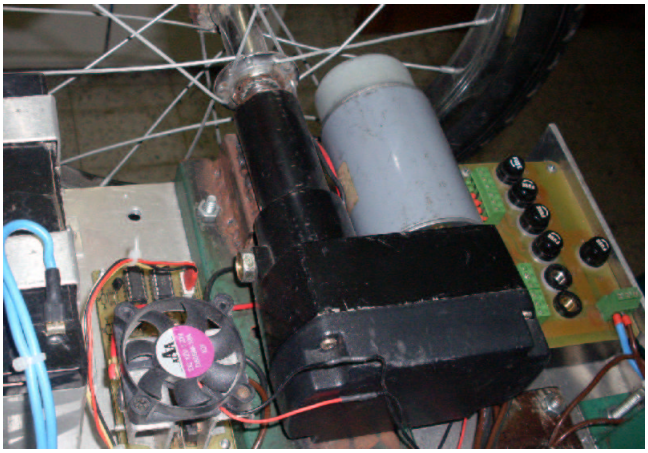

Figure 4.6: Geared motor coupled to the wheels.

### 4.2.2 Motor Driver

Motor H-bridge drivers were required to turn the control signal from the microcontroller into an appropriate varying power level to drive the motors. An H-bridge is an electronic circuit which enables a voltage to be applied across a load in either direction. These circuits are often used in robotics and other applications to allow DC motors to run forwards and backwards. H-bridges are available as integrated circuits, or can be built from discrete components [14].

A "double pole double throw" relay can generally achieve the same electrical functionality as an H-bridge (considering the usual function of the device). Though an H-bridge would be preferable where a smaller physical size is needed, high speed switching, low driving voltage, or where the wearing out of mechanical parts is undesirable. Figure 4.7 shows the structure of the H-Bridge.

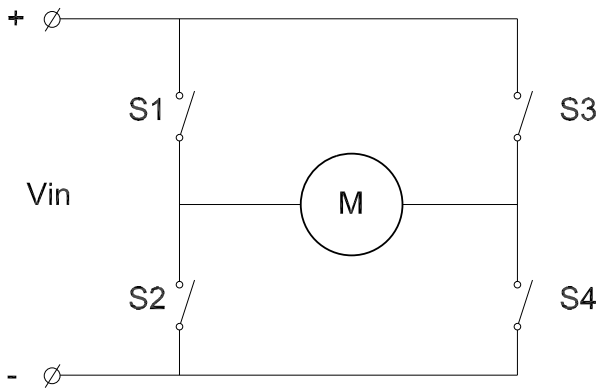


Figure 4.7: Structure of the H-Bridge.

The term "H-bridge" is derived from the typical graphical representation of such a circuit. An H-bridge is built with four switches (solid-state or mechanical). As shown in Figure 4.8, when the switches S1 and S4 (according to the first figure) are closed (and S2 and S3 are open) a positive voltage will be applied across the motor. By opening S1 and S4 switches and closing S2 and S3 switches, this voltage

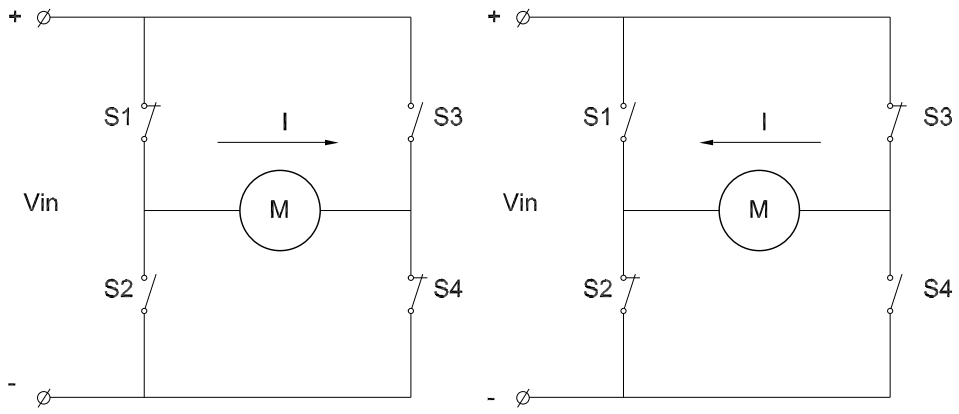


Figure 4.8: Operation of H-Bridge.

is reversed, allowing reverse operation of the motor. Using the nomenclature above, the switches S1 and S2 should never be closed at the same time, as this would cause a short circuit on the input voltage source. The same applies to the switches S3 and S4. This condition is known as shoot-through.

The H-Bridge arrangement is generally used to reverse the polarity of the motor, but can also be used to 'brake' the motor, where the motor comes to a sudden stop, as the motor's terminals are shorted, or to let the motor 'free run' to a stop, as the motor is effectively disconnected from the circuit. Table 4.1 summarizes operation.

Table 4.1: H-Bridge operation .

| S1 | S2 | S3 | S4 | Result |
|---|---|---|---|---|
| 1 | 0 | 0 | 1 | Motor moves right |
| 0 | 1 | 1 | 0 | Motor moves left |
| 0 | 0 | 0 | 0 | Motor free runs |
| 0 | 1 | 0 | 1 | Motor brakes |
| 1 | 0 | 1 | 0 | Motor brakes |

A solid-state H-bridge is typically constructed using reverse polarity devices (i.e., PNP BJTs or P-channel MOSFETs connected to the high voltage bus and NPN BJTs or N-channel MOSFETs connected to the low voltage bus). The most efficient MOSFET designs use N-channel MOSFETs on both the high side and low side because they typically have a third of the ON resistance of P-channel MOSFETs. This requires a more complex design since the gates of the high side MOSFETs must be driven positive with respect to the DC supply rail. Figures 4.9 and 4.10 show the schematic diagram and PCB layout for the implemented H-Bridge FET Driver using P and N-channel MOSFETs.

In this circuit the direction pin (DIR) chooses the direction while the PWM input controls the speed. To turn the motor on full speed set a logic high to the PWM input. Similarly, to turn it off set a logic low. Usually, though, this is not ideal for accurate motor control. Instead, consider a logic low on the direction pin

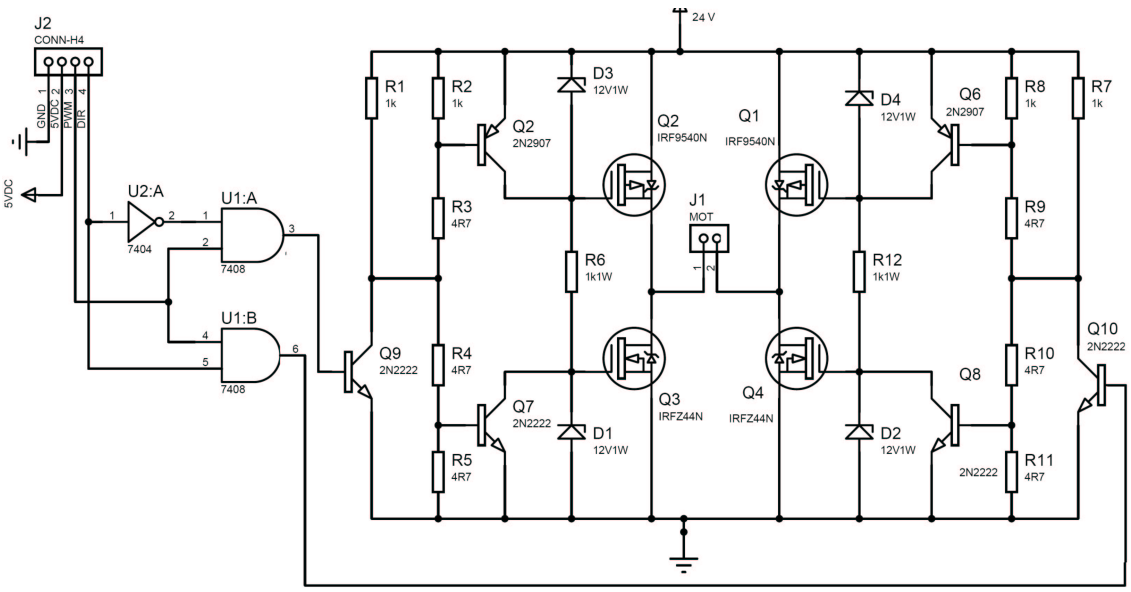


Figure 4.9: Schematic diagram for the designed H-Bridge FET Driver.

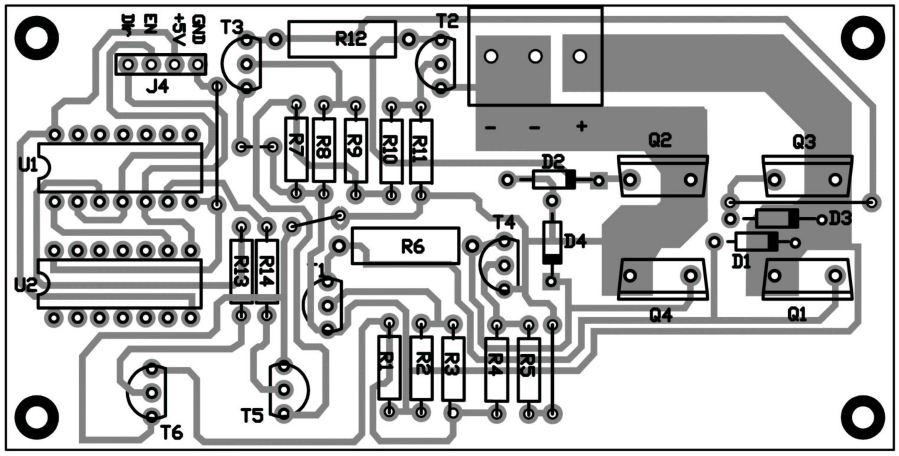


Figure 4.10: H-Bridge FET motor driver PCB layout.

with a 50% duty cycle PWM yields a half reverse speed. Changing the PWM affects the speed at which the motor will turn in reverse while toggling the direction pin changes the direction at which the motor turns. Figure 4.11 shows the implemented H-Bridge FET motor driver view.

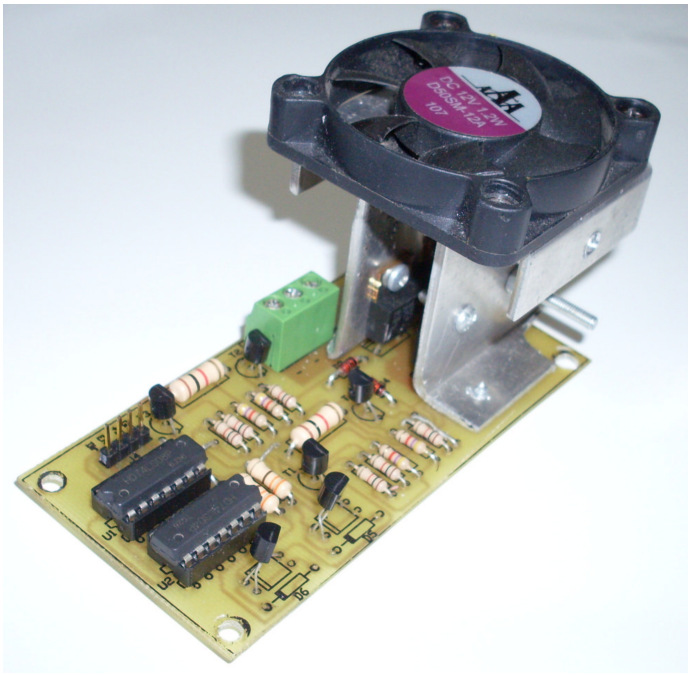

Figure 4.11: H-Bridge FET motor driver view.

### 4.2.3 Microcontroller

The Segway is controlled by a PIC16F877A microcontroller board shown in Figure 4.12. It interfaces with a computer for programming the chip or viewing sensor values in real-time. Note that although a PC is used for debugging, the segway itself is controlled entirely by the microcontroller.

It is protected by a 1A diode to prevent reversing polarity, and a large filter capacitor before the 5V regulator (LM7805). The schematic diagram and PCB layout are shown in Figures 4.13 and 4.14.

- **(J13) Power Entry:** +V could be virtually any DC power source, 7.2V - 24V. For our Segway, power comes from a 24V sealed lead-acid battery.
- **(D1) Reverse Polarity Protection:** A diode only allows current to flow in one direction.
- **(C6 - C1) Power Filters:** A large capacitor between the power supply positive circuit and ground filters out noise from power electronics that control the large motors. Other smaller capacitors provide additional filtering for individual components.

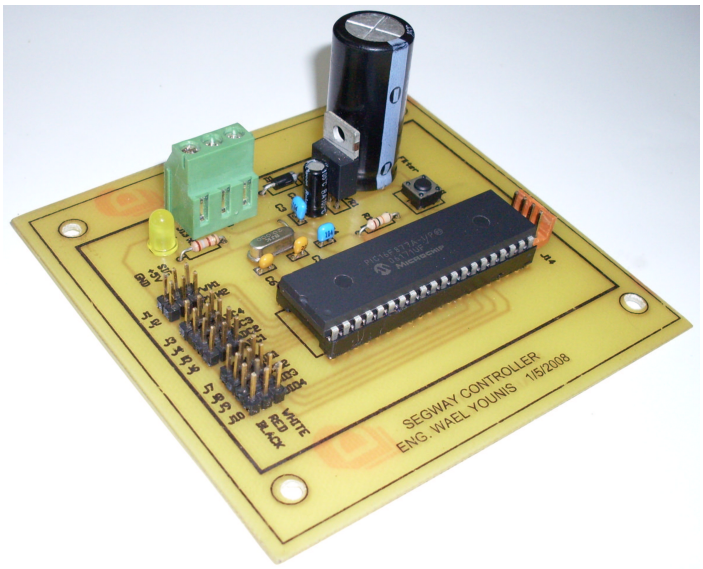


Figure 4.12: View of the microcontroller board.

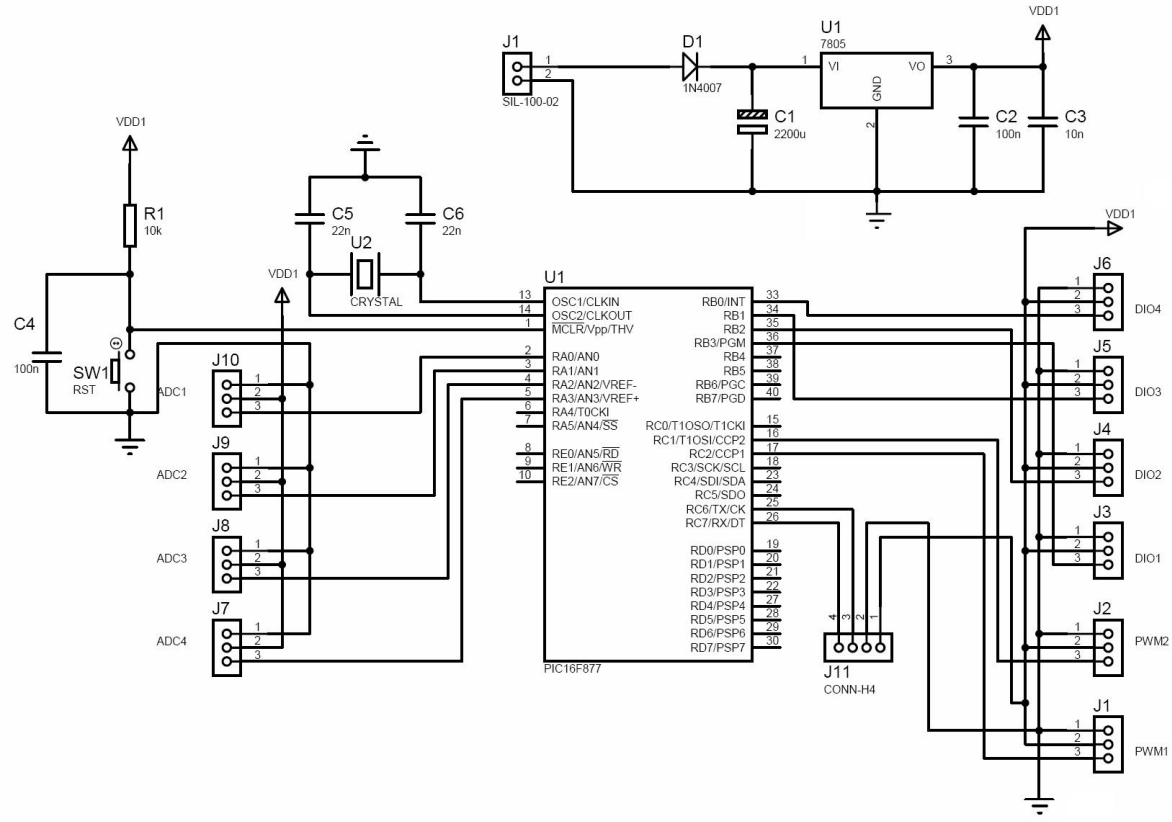


Figure 4.13: The microcontroller board circuit schematic diagram.

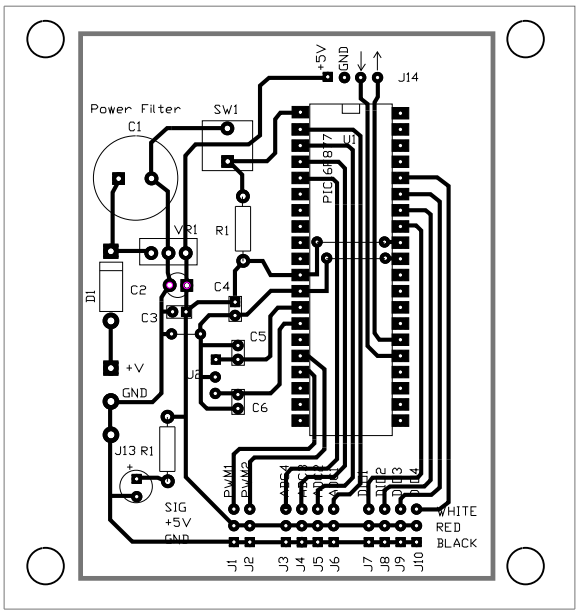


Figure 4.14: The microcontroller board PCB Layout.

- **(VR1) Voltage Regulators:** A 5V regulator (LM7805) takes whatever voltage the battery supplies as its input and output, a smooth 5V for running the microcontroller and sensors.
- **(U1) Microcontroller:** A PIC16F877A microcontroller handles all of the control tasks based on a program that can be written and downloaded onto it.
- **(U2) Oscillator:** A small device that keeps time for the microcontroller. It can run at up to 20MHz, 20 million "ticks" per second.
- **(SW1) Reset:** A button that connects the reset pin of the microcontroller to ground when pushed, causing a reset. Otherwise, the "pull-up" resistor R1 connects the reset pin to 5V, causing it to do nothing.
- **(J1-J2) PWM Outputs:** PWM (Pulse Width Modulation) is the type of signal used to control the motors . These two outputs are connected to specific pins on the microcontroller that can generate 5V pulses with accurately-timed duration (width) of 1-2 milliseconds.
- **(J3-6) Analog Inputs:** Four inputs can be used to read the value of analog sensors. These could be used for steering, additional gyroscopes/accelerometers or potentiometers.
- **(J7-J10) Digital Input/Outputs:** Four digital connections provide a way to read in on/off sensors (switches) or to control on/off devices (LEDs, relays).

The implemented microcontroller board fixed to base plate is shown in Figure 4.15.

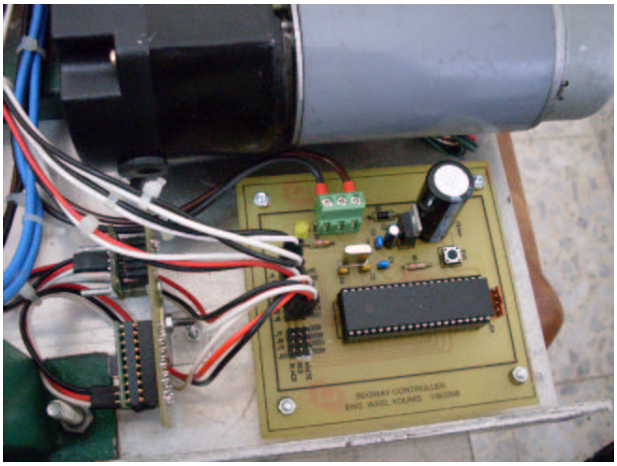

Figure 4.15: The microcontroller board fixed to the base plate.

### 4.2.4 Sensors

The system to balance segway requires the use of three sensors: a gyroscope and an accelerometer for balancing, and a potentiometer for steering measurements . The gyroscope and accelerometer are chosen from the Analog Devices11 iMEMS [9, 10]. They report an analog voltage between 0V and 5V to the controller. The gyroscope is used simply to measure angular rate. The accelerometer is used to indirectly measure the direction of the force of gravity, since it is really sensing force per unit mass along a given axis. This, along with a small angle approximation, gives an estimate of the angle to horizontal . This design needs to have a dual axis high sensitivity accelerometer to detect the angle of tilt on the vehicle.

To determine how fast the vehicle is tipping over, a sensor that detects the rate of change in angular position is vital. Theoretically, this value could be obtained in software by differentiating the reading from the accelerometers, but in reality signals have noise, and noise will quickly destroy a signal resulting from a differentiation, and any filtering would delay the response time of the system, therefore, a dedicated angular rate sensor is the best option.

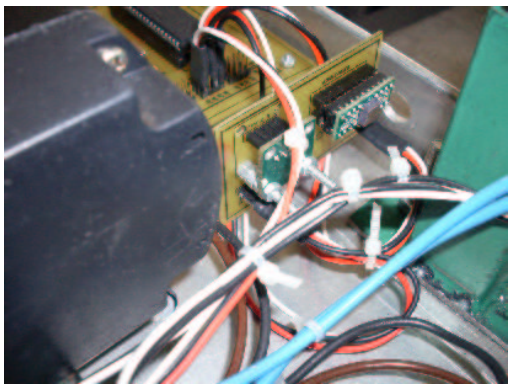

Figure 4.16: The accelerometer and gyroscope board fixed to the base plate.

The Analog Devices accelerometer evaluation board ADXL203EB and the angular rate evaluation board ADXRS401EB are chosen for this research . The implemented accelerometer and gyroscope board fixed to base plate is shown in Figure 4.16. The sensors used in the design and the treatment of sensor information together with experimental results are discussed in detail in Chapter 5.

Steering measurements is obtained using a potentiometer as a proportional control that increases the force exerted on one of the wheels while decreasing it on the other, producing the desired turning. Figure 4.17 shows the chosen potentiometer.

Figure 4.17: Potentiometer for steering measurements.

### 4.2.5 Batteries

The runtime of the segway is dependent on the capacity of the on-board power supply. Batteries are quickly determined to be the simplest way to provide on-board power. The power supply needed to meet the following requirements:

- As compact as possible.
- As light as practical.
- Fast charge rate (minimum recharging time).
- High discharge capacity to cope with high current draw by motor controller.
- Low cost
- Provide sufficient power to the segway for 1 hour

Different types of rechargeable batteries include NiCad, SLA, NiMH, and Li-ion. Nickel Cadmium (NiCad) and Sealed Lead Acid (SLA) have both been around for many years and are well suited to low current drawing applications. The Sealed Lead Acid batteries are chosen for this application having the following specifications:

- Voltage 12V cell charge.
- Capacity = 7Ah.
- Power capacity = 84Wh.
- High discharge current capacity.

Two Sealed Lead Acid (SLA) batteries in a serial configuration provide 24V for the motor controller and motors. DC/DC regulated step-down circuits reduce the 24V supply to 5V for the sensors, controller board, and the steering potentiometer.

An estimate of the runtime that the batteries can provide to the segway has been completed assuming that the motors were running at 75% of their rated speed. This means that the motors each would be consuming 75% of their 55W rated capacity. It should also be noted that the power consumption of the motors is more significant than the other components, and thus they have been omitted from this calculation.

$$P_{Segway} = 2 \times 55W = 110W$$

$$P_{Segway} \times 0.75 = 0.75 \times 110W = 82.5W$$

As the batteries supply 24V, the current draw for 82.5W would be:

$$I_{Segway} = \frac{P_{Segway}}{V_{Segway}} = \frac{82.5}{24} = 3.44A$$

Therefore the estimated running time of the segway at 75% of its permissible speed is:

$$Runtime_{Segway} = \frac{7Ah}{I_{Segway}} = \frac{7Ah}{3.44} \cong 2h$$

This runtime, however, does not take into account disturbances in the system that would be introduced whilst operating. Actual runtime is expected to be less than 2 hours which will be acceptable providing that segway is not driven hard. A photograph of the elected Sealed Lead Acid (SLA) batteries is shown as Figure 4.18.

### 4.2.6 Bearings

Two cylindrical roller bearings have been used on each axle to provide both thrust support against the axle moving relative to the gearbox enclosure, and to transmit vertical loads placed on the platform through to the wheels. The following is a brief calculation used to verify the required capacity of the bearings:

$$M_{Person} = 70kg$$

$$M_{Segway} = 15kg$$

$$M_{Total} = 85kg$$


Figure 4.18: Photograph of the battery used for the segway.

$$F_{Total} = 9.81 \times 85kg = 0.834kN$$

Assuming a safety factor of 2, the maximum load applied to the axles would be about 2kN. Four bearings are used to support the axles, therefore the maximum load applied to each bearing is 0.5kN. The S6002 cylindrical roller bearing is appropriate for use in this application. The S6002 has a dynamic load rating of 4.3kN which is far greater than the expected load of 0.5kN. Figure 4.19 shows a model of the roller bearings. The inner face can be seen to sit against the edge of the rolling cylinders in Figure 4.20, thereby providing the thrust capability of this type of bearing. A shoulder on the axle would then need to press against the inner face of the bearing.

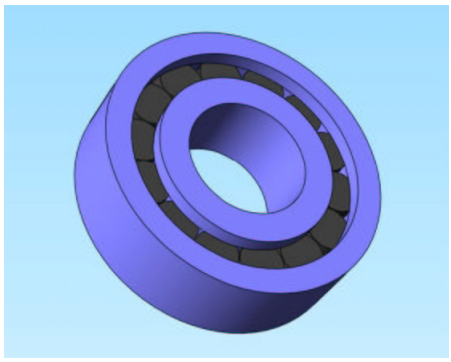

Figure 4.19: Solid Works model of a cylindrical roller ball bearing.

### 4.2.7 Wheels

Aesthetic considerations required the diameter of the wheels to be at least as large as the front-back dimension of the platform, and thus the diameter of the wheels needed to be at least 400mm. A high inertia was a desirable property of the wheels as it allows torque from the motors at low speeds to act on the angle of the platform as well as the speed of the wheels. This means that at low speeds or when

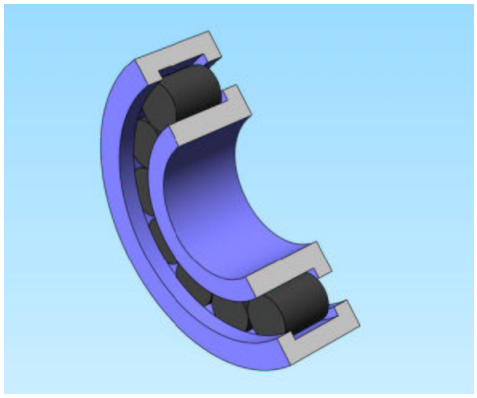

Figure 4.20: Solid Works model of a cylindrical roller ball bearing in cross section.

stationary, small changes in angle from upright results in the motors correcting this angle directly, rather than having to spin the wheels to move them underneath the platform. Bicycle wheels shown in Figure 4.21 with a diameter of 400mm are selected for this application.

Figure 4.21: Selected bicycle wheels with a diameter of 400mm.

# Chapter 5

# The Balance Filter and experimental results

This chapter discusses the sensors used in the design and the treatment of sensor information together with experimental results. Two sensors are used: a gyroscope and an accelerometer for balancing. The sensors are all from the Analog Devices iMEMS line. They report an analog voltage between 0V and 5V to the controller, with neutral angle or zero rate being near 2.5V, although each requires some calibration with regards to the exact offset. The gyroscope is used simply to measure angular rate. The accelerometer is used to indirectly measure the direction of the force of gravity, since it is really sensing force per unit mass along a given axis. This, along with a small angle approximation, gives an estimate of the angle to horizontal.

## 5.1 Microelectromechanical systems (MEMS)

In this section description and applications of Microelectromechanical technology is discussed.

### 5.1.1 Microelectromechanical systems description

Microelectromechanical systems (MEMS) (also written as micro-electro-mechanical, or MicroElectroMechanical) is the technology of the very small, and merges at the nano-scale into nanoelectromechanical systems (NEMS) and nanotechnology. MEMS are also referred to as micromachines (in Japan), or Micro Systems Technology - MST (in Europe). MEMS are separate and distinct from the hypothetical vision of Molecular nanotechnology or Molecular Electronics. MEMS are made up of components between 1 to 100 micrometers in size (i.e. 0.001 to 0.1 mm) and MEMS devices generally range in size from 20 micrometers (20 millionths of a meter) to a millimeter. They usually consist of a central unit that processes data, the microprocessor and several components that interact with the outside such as microsensors [15]. At these size scales, the standard constructs of classical physics do not always hold true. Due to MEMS' large surface area to volume ratio, surface

effects, such as electrostatics and wetting dominate volume effects such as inertia or thermal mass. MEMS technology can be implemented using a number of different materials and manufacturing techniques; the choice of which will depend on the device being created and the market sector in which it has to operate.

### 5.1.2 Applications

Commercial applications of MEMS include:

- Inkjet printers, which use piezoelectrics or thermal bubble ejection to deposit ink on paper.
- Accelerometers in modern cars for a large number of purposes including airbag deployment in collisions.
- Accelerometers in consumer electronics devices such as game controllers (Nintendo Wii), personal media players / cell phones (Apple iPhone ) and a number of Digital Cameras (various Canon Digital IXUS models). Also used in PCs to park the hard disk head when free-fall is detected, to prevent damage and data loss.
- MEMS gyroscopes used in modern cars and other applications to detect yaw; e.g. to deploy a roll over bar or trigger dynamic stability control.
- Silicon pressure sensors e.g. car tire pressure sensors, and disposable blood pressure sensors.
- Displays e.g. the DMD chip in a projector based on DLP technology has on its surface several hundred thousand micromirrors.
- Optical switching technology which is used for switching technology and alignment for data communications.
- Bio-MEMS applications in medical and health related technologies from Lab-On-Chip to Micro Total Analysis (biosensor, chemosensor).
- Interferometric modulator display (IMOD) applications in consumer electronics (primarily displays for mobile devices). Used to create interferometric modulation - reflective display technology as found in mirasol displays.

## 5.2 Gyroscope and Accelerometer

In this design two sensors are used, accelerometer and gyroscope. The gyroscope is used simply to measure angular rate and The accelerometer is used for angle estimation to horizontal.

### 5.2.1 Dual axis accelerometer (ADXL203)

The ADXL203 is high precision, low power, complete dual axis accelerometer with signal conditioned voltage outputs, all on a single monolithic IC [9]. The ADXL203 contains a polysilicon surface-micromachined sensor and signal conditioning circuitry to implement an open-loop acceleration measurement architecture. The output signals are analog voltages proportional to acceleration. The ADXL203 are capable of measuring both positive and negative accelerations to at least 1.7 g. The accelerometer can measure static acceleration forces such as gravity, allowing it to be used as a tilt sensor. The sensor is a surface-micromachined polysilicon structure built on top of the silicon wafer. Polysilicon springs suspend the structure over the surface of the wafer and provide a resistance against acceleration forces. Deflection of the structure is measured using a differential capacitor that consists of independent fixed plates and plates attached to the moving mass. The fixed plates are driven by 180 out-of-phase square waves. Acceleration will deflect the beam and unbalance the differential capacitor, resulting in an output square wave whose amplitude is proportional to acceleration. Phase sensitive demodulation techniques are then used to rectify the signal and determine the direction of the acceleration. The output of the demodulator is amplified and brought off-chip through a 32 k. resistor. At this point, the user can set the signal bandwidth of the device by adding a capacitor. This filtering improves measurement resolution and helps prevent aliasing. Figure 5.1 shows the functional diagram of ADXL203.

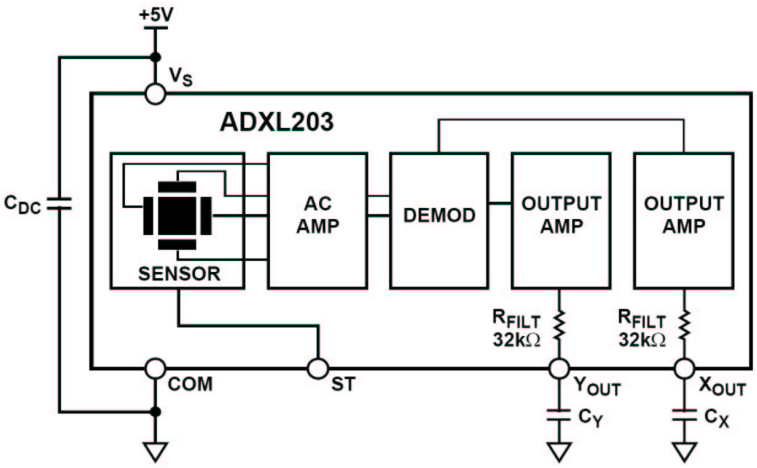


Figure 5.1: Accelerometer (ADXL203) functional block diagram.

ADXL203 dual axis 1.7 g accelerometer has the following features :

- High performance, single/dual axis accelerometer on a single IC chip.
- 1 mg resolution at 60 Hz.
- Low power: 700 $\mu$A at $V_S$=5 V(typical).
- High zero g bias stability accuracy.
- High sensitivity.

- -40C to +125C temperature range.
- X and Y axes aligned to within 0.1° (typical).
- 3500 g shock survival

The accelerometer evaluation board ADXL203EB from Analog Devices is chosen due to its 5V operating voltage, high sensitivity, and simple pin out. The ADXL203EB is a simple evaluation board that allows quick evaluation of the performance of the ADXL203 dual axis 1.7 g accelerometer.The schematic of the ADXL203EB the board view are shown in Figures 5.2 and 5.3. Analog bandwidth can be set by changing capacitors C2 and C3.

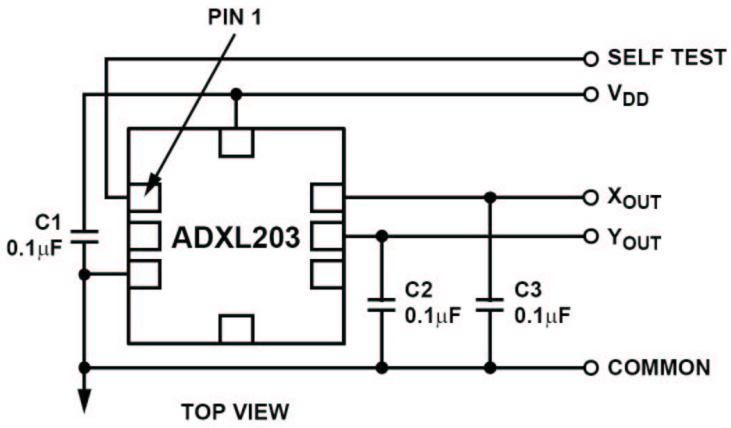


Figure 5.2: The schematic of the ADXL203EB evaluation board.

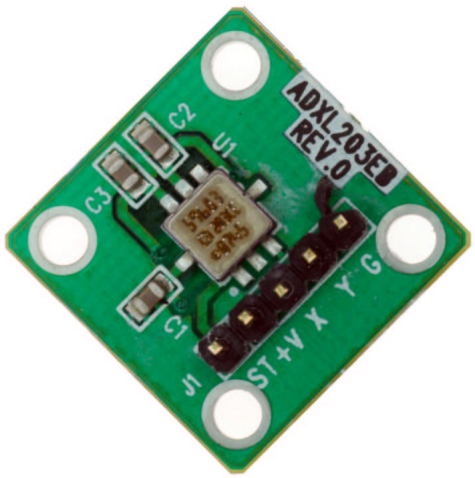


Figure 5.3: View of ADXL203EB evaluation board.

### 5.2.2 Gyroscope (ADXRS401)

The ADXRS401 is a functionally complete and low cost angular rate sensor (gyroscope), integrated with all of the required electronics on one chip [10]. The output

signal, rateout (1B, 2A), is a voltage proportional to angular rate about the axis normal to the top surface of the package (see Figure 5.4).

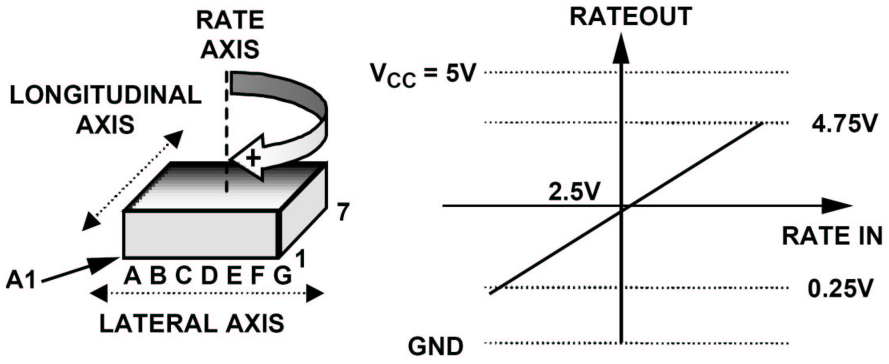


Figure 5.4: Rateout signal increases with clockwise rotation.

The gyroscope (ADXRS401) operates on the principle of a resonator gyro. Two polysilicon sensing structures each contain a dither frame, which is electrostatically driven to resonance. This produces the necessary velocity element to produce a Coriolis force during angular rate. At two of the outer extremes of each frame, orthogonal to the dither motion, are movable fingers that are placed between fixed pickoff fingers to form a capacitive pickoff structure that senses Coriolis motion. The resulting signal is fed to a series of gain and demodulation stages that produce the electrical rate signal output. The dual-sensor design rejects external g-forces and vibration. Fabricating the sensor with the signal conditioning electronics preserves signal integrity in noisy environments. The electrostatic resonator requires 14 V to 16 V for operation. Since only 5 V is typically available in most applications, a charge pump is included on-chip. If an external 14 V to 16 V supply is available, the two capacitors on CP1 to CP4 can be omitted and this supply can be connected to CP5 (Pin 7D) with a 1 $\mu$F decoupling capacitor. After the demodulation stage there is a single-pole low-pass filter consisting of an internal 9 k$\Omega$ resistor ($R_{SEN1}$) and an external user-supplied capacitor (CMID). A CMID capacitor of 100 nF sets a 400 Hz low-pass pole $\pm$ 0.35 and is used to limit high frequency artifacts before final amplification. A bandwidth limit capacitor, $C_{OUT}$, sets the pass bandwidth. Figure 5.5 shows the functional diagram of ADXRS401.
The ADXRS401ABG yaw rate gyro has the following features :

- Complete rate gyroscope on a single chip.
- Z-axis (yaw-rate)response.
- High vibration rejection over wide frequency.
- 2000 g powered shock survivability.
- Self-test on digital command.
- Absolute rate output for precision applications.
- 5 V single-supply operation.

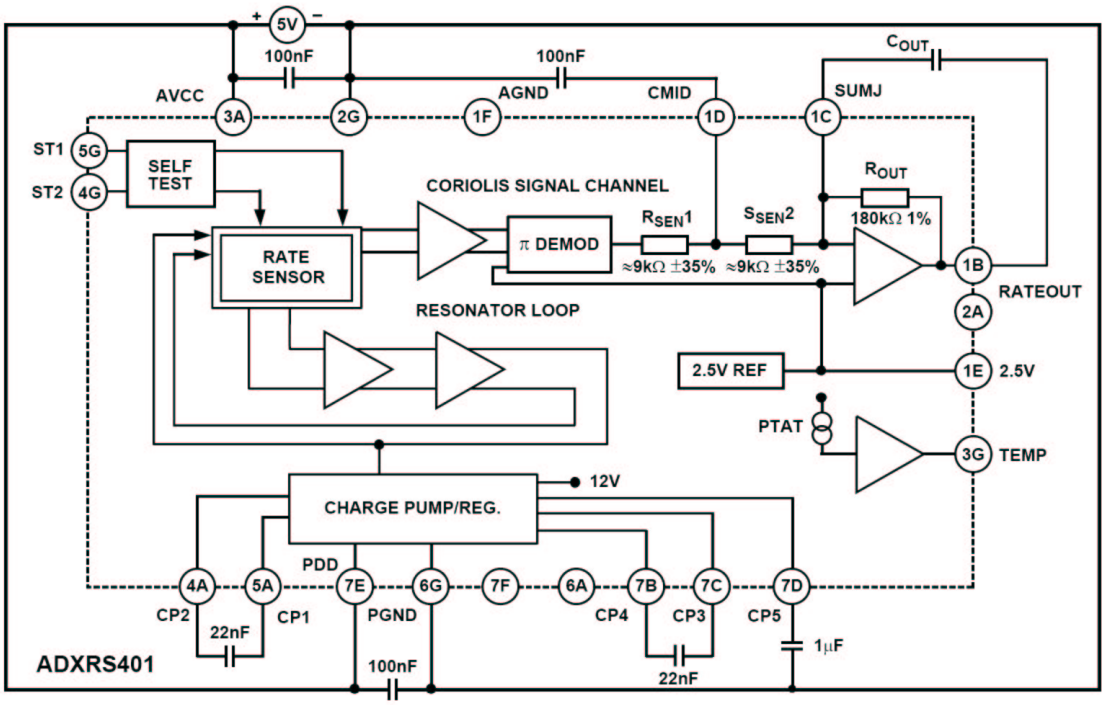


Figure 5.5: Gyroscope (ADXRS401) functional block diagram.

The gyroscope evaluation board ADXRS401EB from Analog Devices is chosen for this research. The ADXRS401EB is a simple evaluation board that allows the user to quickly evaluate the performance of the ADXRS401ABG yaw rate gyro. The schematic of the ADXRS401EB and the board view are shown in Figures 5.6 and 5.7.

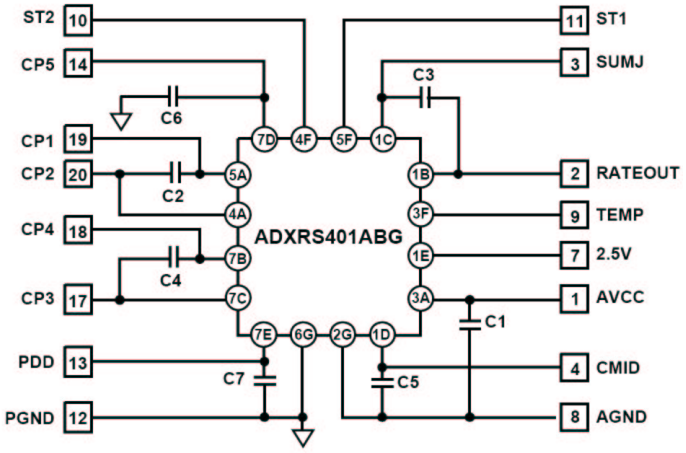


Figure 5.6: The schematic of the ADXRS401EB evaluation board.

Figure 5.7: View of ADXRS401EB evaluation board.

## 5.3 The Balance Filter and experimental results

In order to control the platform, it must be known that both the angle and the angular velocity of the base platform. This should be the basis for an angle PD (proportional/derivative) control algorithm, which has been proven to work well for this type of system [3].

$$MotorOutput = K_p(Angle) + K_d(AngularVelocity) \tag{5.1}$$

Thus it is very important to get a clean, fast angle estimate which will be implemented using accelerometer and gyroscope. There are a number of problems with using direct sensor data for control. For one, with electric motors on the same power and ground line as the controller, there is bound to be noise in the system even with a power supply filter capacitor for the controller. There are also physical reasons why the data from the accelerometers and gyroscope has to be filtered. The accelerometers measure a change in angle by the component of the force of gravity along their sensitive axis (horizontal). But they also report other horizontal accelerations from the motors. The gyroscope measures angular rate and can be used to estimate angle by integration. But this method can lead to drift. The tow axis accelerometer measures acceleration, but really force per unit mass and can be used to measure the force of gravity. Above, X-axis reads 0g, Y-axis reads -1g (Figure 5.8). For a balancing platform, the most important angles to measure are near vertical. If the platform tilts more than 30 degrees in either direction, theres probably not much the controller can do other than drive full speed to try to catch it. Within this window, one can use small angle approximation and the X-axis to save processor time and coding complexity. If the platform is tilted forward by an angle $\theta$, but stationary (not accelerating horizontally), X-axis reads: $(1g) \times sin(\theta)$, for the small angle approximation $sin(\theta) = (\theta)$ in radians.

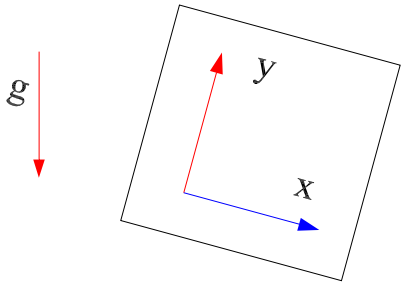


Figure 5.8: Measuring the force of gravity above x and y axis.

The first step is to read in analog inputs (through the analog-to-digital converter, ADC) for each sensor and get them into useful units. This requires adjustment for offset and scale. The offset is found by seeing what integer value the sensor reads when it is horizontal and/or stationary. If it flickers around, we choose an average value. The scale depends on the sensor. It is the factor by which to multiply to get the desired units.

*Acc.=(Acc.ADC-Acc.ADC offset) × Acc.ADC scale*
*Gyro=(Gyro ADC-Gyro ADC offset) × Gyro ADC scale*

### 5.3.1 Maping Sensors

The most obvious method to estimate the angle and the angular velocity is the direct reading method, which depends on the accelerometer to obtain the angle and the gyroscope to obtain the angular velocity. A block diagram of this method is shown in Figure 5.9

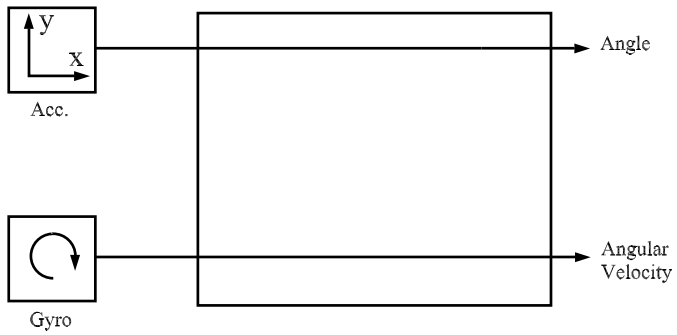


Figure 5.9: A block diagram of direct reading method.

This metod is intuitive and easy to code and the Gyro gives fast and accurate angular velocity measurement. On the other hand, it is noisy because the accelerometer will read any horizontal acceleration in X-axis as a change in angle. (Imagine the platform is horizontal, but the motors are causing it to accelerate forward. The accelerometer cannot distinguish this from gravity).

Adding a low-pass filter on the accelerometer estimated angle (Figure 5.10) will filter out short-duration horizontal accelerations and only long-term acceleration (gravity) passes through. This could be as simple as averaging samples:

$$angle = (0.75) \times (angle) + (0.25) \times (x_{acc}) \tag{5.2}$$

0.75 and 0.25 are example values. These could be tuned to change the time constant of the filter as desired. But in this case the angle measurement will lag due to the averaging.

The other approach to estimate the angle and the angular velocity is to use only one sensor (Gyroscope) as shown in Figure 5.11.
The integration could be accomplished in code like :

$$angle = angle + gyro \times dt \tag{5.3}$$

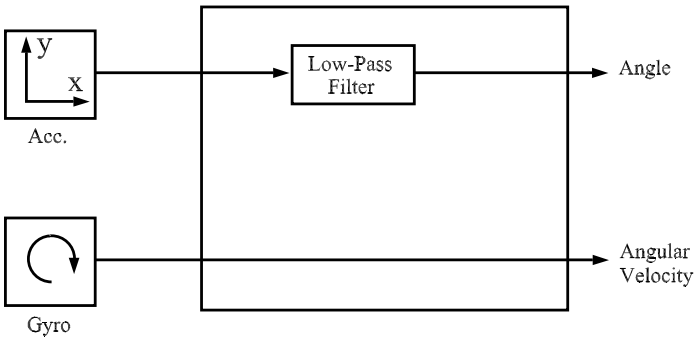


Figure 5.10: A block diagram of the system with low-pass filter on the accelerometer.

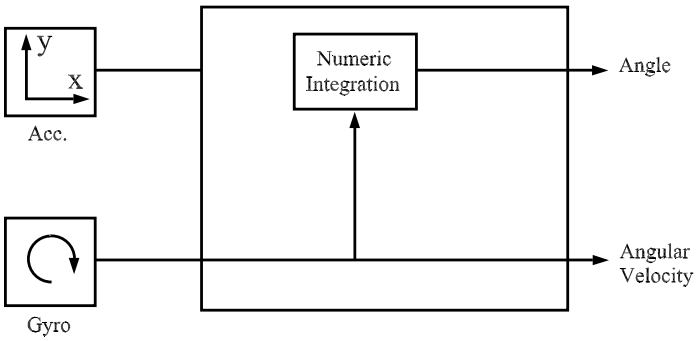


Figure 5.11: A block diagram of the system using only the gyroscope.

This requires that one knows the time interval between updates (dt). This approach used only one sensor to read so it is fast and lag is not a problem. On the other, hand the dreaded gyroscopic drift. If the gyro does not read perfectly zero when stationary (and it wont), the small rate will keep adding to the angle until it is far away from the actual angle. To solve the previous problems a simple software filter has been developed. This filter is shown in Figure 5.12.

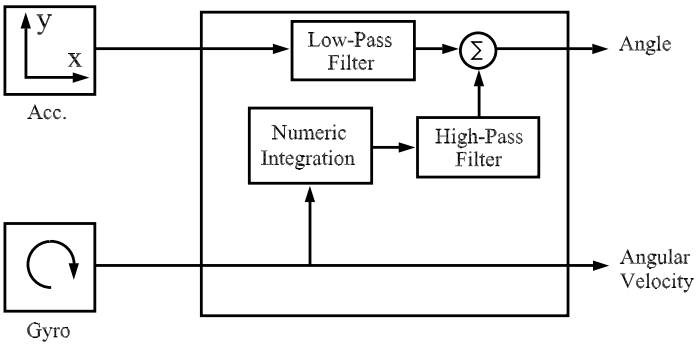


Figure 5.12: A block diagram of the system using complementary filter.

This filter can help fix noise, drift, and horizontal acceleration dependency. The angle estimate is fast and much less lag than low-pass filter alone, and it is not very processor intensive.

### 5.3.2 More on Digital Filters

In electronics, computer science and mathematics, a digital filter is a system that performs mathematical operations on a sampled, discrete-time signal to reduce or enhance certain aspects of that signal. In this subsection some filter types is presented.

#### Integration

Think of a car traveling with a known speed and your program is a clock that ticks once every few milliseconds. To get the new position at each tick, you take the old position and add the change in position. The change in position is just the speed of the car multiplied by the time since the last tick, which you can get from the timers on the microcontroller or some other known timer. In code:

$$position+ = speed \times dt \tag{5.4}$$

or for a balancing platform,

$$angle+ = gyro \times dt \tag{5.5}$$

#### Low-Pass Filter

The goal of the low-pass filter is to only let through long-term changes, filtering out short-term fluctuations. One way to do this is to force the changes to build up little by little in subsequent times through the program loop. In code:

$$angle = (0.98) \times angle + (0.02) \times x_{acc} \tag{5.6}$$

If, for example, the angle starts at zero and the accelerometer reading suddenly jumps to 10, the angle estimate changes as shown in Table 5.1 in subsequent iterations:

Table 5.1: The angle estimate via low-pass filters.

| Iter. | 1 | 2 | 3 | 4 | 5 | 6 | 7 | 8 | 9 | 10 |
|---|---|---|---|---|---|---|---|---|---|---|
| $\theta$ | 0.20 | 0.40 | 0.59 | 0.78 | 0.96 | 1.14 | 1.32 | 1.49 | 1.66 | 1.83 |

If the sensor stays at 10°, the angle estimate will rise until it levels out at that value. The time it takes to reach the full value depends on both the filter constants (0.98 and 0.02 in the example) and the sample rate of the loop (dt).

#### High-Pass Filter

Conceptually the high pass filter does the exact opposite of the low pass filter. It allows short-duration signals to pass through while filtering out signals that are steady over time. This can be used to cancel out drift.

**Sample Period:**

Is the amount of time that passes between each program loop complete. If the sample rate is 100 Hz, the sample period is 0.01 sec.

**Time Constant:**

The time constant of a filter is the relative duration of signal it will act on. For a low-pass filter, signals much longer than the time constant pass through unaltered while signals shorter than the time constant are filtered out. The opposite is true for a high-pass filter. The time constant, $\tau$, of a digital low-pass filter,

$$y = (a) \times angle + (1 - a) \times x \tag{5.7}$$

running in a loop with sample period, dt, can be found like this:

$$\tau = \frac{a.dt}{1 - a} \Longleftrightarrow a = \frac{\tau}{\tau + dt} \tag{5.8}$$

Therefore knowing the desired time constant and the sample rate, the filter coefficient is determined.

### 5.3.3 A Closer Look at the Implemented Angle Filter

The first part of this filter resembling a high-pass filter on the integrated gyro angle estimate. It will have approximately the same time constant as the low-pass filter. The second is a low-pass portion acting on the accelerometer.

$$angle = (0.98) \times (angle + gyro \times dt) + (0.02) \times (acc) \tag{5.9}$$

If this filter was running in a loop that executes 100 times per second, the time constant for both the low-pass and the high-pass filter would be:

$$\tau = \frac{a.dt}{1 - a} = \frac{0.98 \times 0.01}{0.02} = 0.49 \tag{5.10}$$

This defines where the boundary between trusting the gyroscope and trusting the accelerometer is. For time periods shorter than half a second, the gyroscope integration takes precedence and the noisy horizontal accelerations are filtered out. For time periods longer than half a second, the accelerometer average is given more weighting than the gyroscope, which may have drifted by this point. For the most part, designing the filter usually goes the other way. First, one picks a time constant and then uses that to calculate filter coefficients. Picking the time constant is the place where you can tweak the response. If your gyroscope drifts on average 2 per second (probably a worst-case estimate), you probably want a time constant less than one second so that you can be guaranteed never to have drifted more than a couple degrees in either direction. But the lower the time constant, the more horizontal acceleration noise will be allowed to pass through. Like many other control situations, there is a tradeoff and the only way to really tweak it is to experiment.

Remember that the sample rate is very important to choosing the right coefficients. If one changes the program, adding a lot more floating point calculations, and your sample rate goes down by a factor of two, the time constant will go up by a factor of two unless one recalculate the filter terms. As an example, consider using the 26.2 msec as a control loop time. If a time constant of 0.75 sec is wanted, the filter term would be:

$$a = \frac{\tau}{\tau + dt} = \frac{0.75sec}{0.75sec + 0.0262sec} = 0.966 \tag{5.11}$$

So,

$$angle = (0.966) * (angle + gyro * 0.0262) + (0.02) * (acc). \tag{5.12}$$

The second filter coefficient, 0.034, is just (1 - 0.966). Some experimental results are shown in Figure 5.13.

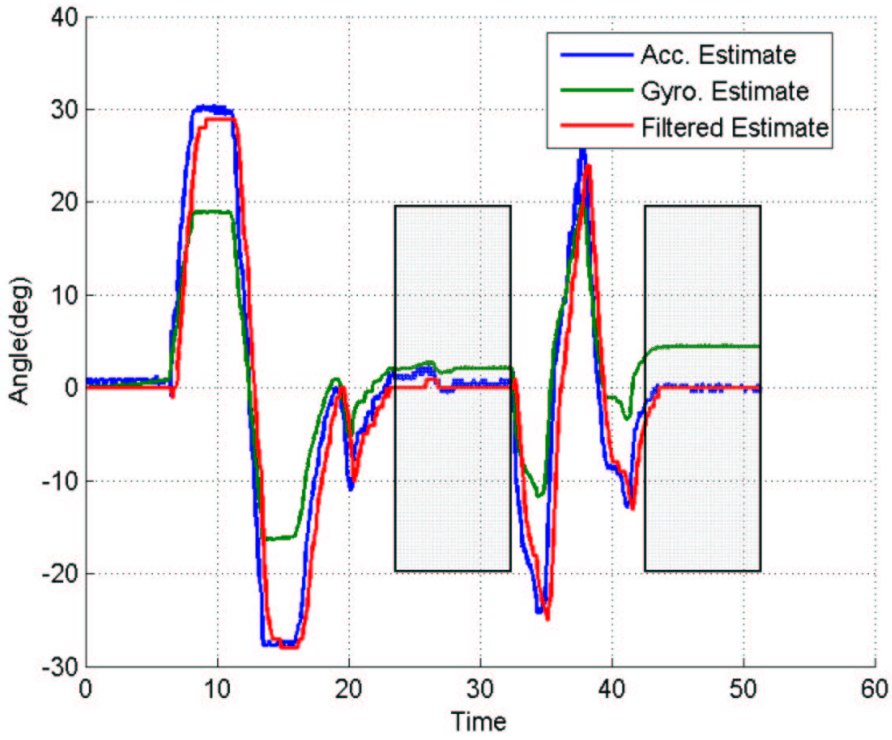


Figure 5.13: Experimental results for Sample Rate of 98 Hz and filter Coefficients of 0.98 and 0.02.

This results is obtained for, a sample rate of 79 Hz, filter Coefficients of 0.98 and 0.02 and time constant of 0.62 sec. Notice how the filter handles both problems, horizontal acceleration disturbances while not rotating and gyroscope drift.

Having completed the controller design, a set of experimental results is made. This allows to check its operation and to fine-tune the parameters of the controller. The signal that comes from the controller, corresponding to the force to apply to the cart, is spread in a symmetric way between the two wheels of the vehicle. Moreover, steering is obtained using a proportional control that increases the force exerted on one of the wheels while decreasing it on the other, producing the desired turning. Figures 5.14 and 5.16 show the response of the system for different initial tilt angles.

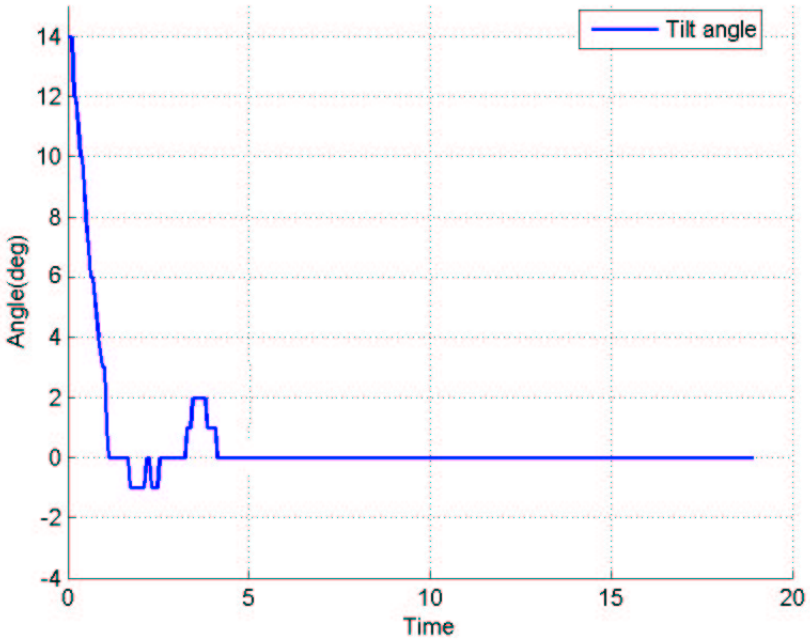


Figure 5.14: Response for initial tilt angle of 14 deg.

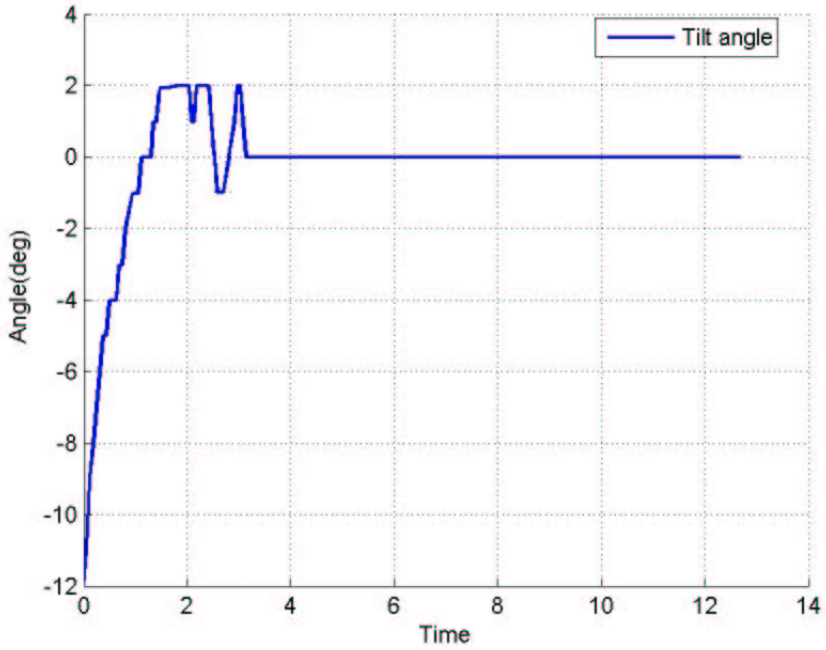


Figure 5.15: Response for initial tilt angle of -12 deg.

# Chapter 6

# Conclusions and Suggestions

## 6.1 Research review

As a result of this experimental research, a segway whose behavior is based on the stabilization of an inverted pendulum was presented. This vehicle has been manufactured using low-cost commercial components. An experimentation system has been obtained and allows to test various controllers. The model has been tested for its balance by running a Proportional Derivative (PD) algorithm on a microprocessor chip. The model has been identified in order to serve as an educational experimental platform for segways. Future developments will include designing new control techniques and performing a comparative study among them. This work has succeeded in achieving its aims to balance a two-wheeled Segway based on the inverted pendulum model.

The controller shows promising results in balancing the Segway. During testing, the Segway is able to maintain its vertical position by slightly adjusting its wheels.

The angle Filter has been successfully implemented. The gyroscope drift and horizontal acceleration disturbances of the accelerometer have been effectively eliminated allowing for an accurate estimate of the tilt angle and its derivative for the robot.

More research is needed to investigate the effects of linearizing the dynamics of the system mode to improve the stability and robustness of the system. An attempt to control the system using nonlinear methods is highly recommended for future research. That way, oscillatory movements of the vehicle while balancing can be eliminated, thus more robustness can be achieved.

## 6.2 Recommendations for future work

This thesis provides the base for future research on filter applications and control systems development in balancing two wheeled vehicles. More research should be conducted to exploit the filter technology and its application for other projects that require sensor fusion technology. The linear control system developed in this thesis proved to be able to balance the vehicle under minimal disturbance. But, the

robustness of the system is not fully tested and is in question. More experiments needs to be performed to evaluate the robustness of the system and fine tuning of the control algorithm is required for better performance. Future research on implementing non-linear controllers is strongly recommended for the balancing system as it will improve the robustness of the system.

# Bibliography


[1] Segway, Inc. , Last accessed December. 2009. URL:*http://www.segway.com.*

[2] Grasser F, D'Arrigo A, Colombi S and Rufer A. JOE: A mobile inverted pendulum. *IEEE Trans Industrial Electronics* 49(1):107114.

[3] Blackwell, T. , How To Build A Self Balancing Scooter, Last accessed Feb. 2009. URL:*http://tlb.org/scooter.html.*

[4] Beckwith et al. Human Transport Vehicle (HTV). *Project Final Report.* Camosun College, Canada, 2004.

[5] Chudleigh, M., Clarke, D., Lemire-Elmore. The Almost Self Balancing Two Wheeled Electric Skateboard, Last accessed March. 2009. URL:*http://www.ebikes.ca/projects/Emanual/.*

[6] Baloh, M. and M. Parent . Modeling and model verification intelligent self-balancing two-wheeled vehicle for an autonomous urban transportation system. In: *The Conference on Computational Intelligence, Robotics, and Autonomous Systems.* Dec. 15 2003, Singapore.

[7] Control Tutorials for MATLAB and Simulink, Last accessed April 2009. URL:*http://www.library.cmu.edu/ctms/.*

[8] Microchip Technology Inc., PIC16F87XA Datasheet, Last accessed April. 2009. URL:*http://ww1.microchip.com/downloads/en/DeviceDoc/39582b.pdf*

[9] Analog Devices, Inc., ADXL103/ADXL203 Datasheet,Last accessed April 2009. URL:*http://www.analog.com/static/imported-files/data-sheets/ADXL103-203.pdf*

[10] Analog Devices, Inc., ADXRS401 Datasheet, Last accessed April 2009. URL:*http://www.analog.com/static/imported-files/data-sheets/ADXRS401.pdf*.

[11] Wael Younis, Abdelati Muhammed, Design and Implementation of An Experimental Segway Model, *AIP Conference Proceedings, the proceedings of the CISA'09 conference*, Vol.1107, Tunisia, 23 25 March 2009.

[12] M. Fiacchini et al. Design and experimentation of a personal pendulum vehicle. In: *Control, 7th Portuguese Conference on Automatic Control*. 11-13 September 2006. Lisboa, Portugal.

[13] DIY Segway , Last accessed Feb. 2009. URL:*http://web.mit.edu/first/segway*.

[14] Mohammad H. Rashid, Power Electronics Circuits, Devices and Applications, Prentice-Hall International, Second edition, 1993.

[15] Waldner, Jean-Baptiste. Nanocomputers and Swarm Intelligence. London: ISTE John Wiley and Sons. pp. p205. ISBN 1847040020, 2005

[16] Wikipedia, List of moments of inertia, Last accessed Jan. 2009. URL:*http://www.len.wikipedia.org/wiki/List-of-moments-of-inertia*

[17] D. Halliday, R. Resnick and J. Walker, Fundamental of physics, John wiley and sons, INC. 1997.

[18] Astrom, K. J. and K. Furuta . Swinging-up a pendulum by energy control. In: *Proc. IFAC 13th World Congress, San Francisco, California, 1996.* pp. 37-95.

[19] Furuta, K.. Control of pendulum: From super mechano-system to human adaptative mechatronics. In: *Decision and Control. Proceedings. 42nd IEEE Conference.* 9-12 Dec. 2003 .

[20] Gordillo, F., F. Salas and J. Aracil . A forwarding controller for the pendulum on a cart. In:*Proceedings of Control.* Vol. 6. Portugal, 2004.

[21] Franklin G., Powell J.D., Feedback Control of Dynamic Systems, Prentice-Hall International, Fourth edition, 2002.

[22] Ogata K., Modern Control Engineering , 2nd ed., Prentice Hall, NJ, 1990.

[23] Kuo B.C., Automatic Control Systems, 6th ed., Prentice Hall, NJ, 1991.

[24] Astrom K.J., Hagglund I., PID Controllers Theory, Design and Tuning, 2nd edition, ISA, Research Triangle Park, N.C., U.S.A, 1995.

[25] Browning, B. Rybski, P.E. Searock, J. Veloso, M.M., Development of a soccer-playing dynamically-balancing mobile robot ,*Robotics and Automation, 2004. Proceedings. ICRA '04. 2004 IEEE International Conference*, Volume 2, Page(s):1752 - 1757, Apr 26-May 1, 2004.

[26] Voth, D., Segway to the future (autonomous mobile robot) *Intelligent Systems, IEEE*, Volume 20, Issue 3, Page(s):5 - 8, May-June 2005.

# Appendix A

# Calculating and Measuring Parameters for Mathematical Model

**Constant of the motors back EMF,** $k_e$

According to equation (2.2), $k_e = \frac{V_e}{\omega}$. When the motor is running under 24VDC the speed ($n_m$) is 2368 rpm. Therefore,

$$k_e = \frac{V_e}{\omega} = \frac{V_e \times 60}{n_m \times 2\pi} = \frac{24 \times 60}{2368 \times 2\pi} = 0.097 V/rad$$

**Constant of the motors torque** $k_m$

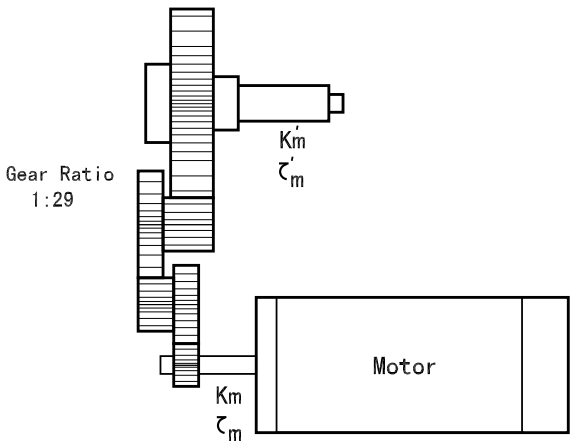


Figure A.1: DC motor and gear box.

At the edge of the gear shaft the constant of the torque is,

$$k_m = 0.0298 Nm/A$$

At the edge of the motor shaft the constant of the torque is,

$$k_m^{'} = 0.0298 \times 29 = 0.864 Nm/A$$

**Length to the body's center of mass**

Assume that the rider of the segway has a 1.7 m high. So the approximate length to the body's center of mass may be,

$$l = 0.8m$$

**Resistance of the armature of motor R**

$$R = 1.0\Omega.$$

**Mass of the pendulum $M_p$**

Assume that the rider (70kg) and the chassis (15kg), system is an ideal pendulum which has all mass at center of gravity. This system weights

$$M_p = 85kg$$

**Wheel radius r**

$$r = 0.2m.$$

**Mass of the wheel $M_w$**

The mass of the wheel is,

$$M_w = 3.5kg$$

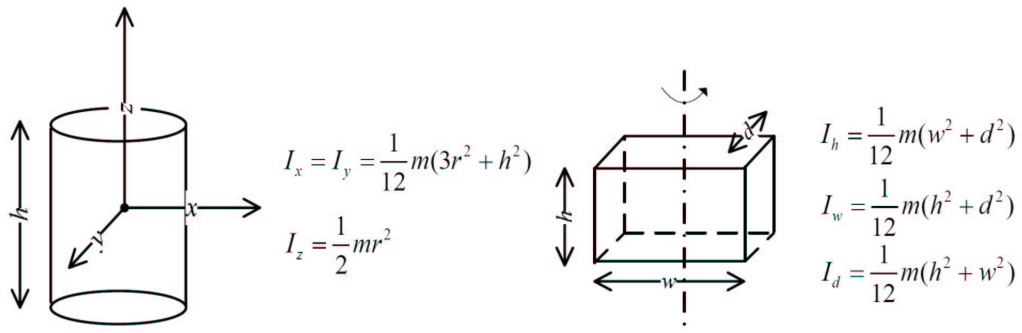


Figure A.2: Moment of inertia of cylinder and cube.

**The moment of inertia of the pendulum $I_p$**

The following equations are used to obtained Moment of inertia of cylinder and cube [16].

Since the pendulum (The rider and chassis system) rotates against the bottom of the cylinder, not against the center of gravity, so the equation

$$I_x = \frac{1}{12}m(3r^2 + h^2)$$

has to be transformed by shifting x-axis to the bottom of the cylinder. According to the parallel-axis theorem, the rotational inertia of a body about any axis is equal to the rotational inertia($Mh^2$) about that axis if all its mass were concentrated at its centre of mass, plus its rotational inertia ($I_{CM}$) about a parallel axis through its center of mass [17].

Therefore,

$$I = I_{CM} + Mh^2$$

M is the mass of the cylinder and h is the perpendicular distance between the two parallel axes.

$$I_{p1} = \frac{1}{12}m(3r^2 + h^2) + m(\frac{h}{2})^2 = \frac{1}{12}M_{p1}(3r^2 + h^2) + M_{p1}(\frac{h}{2})^2$$

$$I_{p1} = \frac{70kg}{12}(3 \times 0.15^2 + 1.7^2) + 70kg(\frac{1.7}{2})^2 = 67.827kg.m^2$$

$$I_{p2} = \frac{1}{12}m(3h^2 + d^2) + m(\frac{h}{2})^2 = \frac{1}{12}M_{p2}(3h^2 + d^2) + M_{p2}(\frac{h}{2})^2$$

$$I_{p2} = \frac{15kg}{12}(3 \times 0.12^2 + 0.37^2) + 15kg(\frac{0.12}{2})^2 = 0.243kg.m^2$$

$$I_p = I_{p1} + I_{p2} = 67.83 + 0.243 = 68.07g.m^2$$

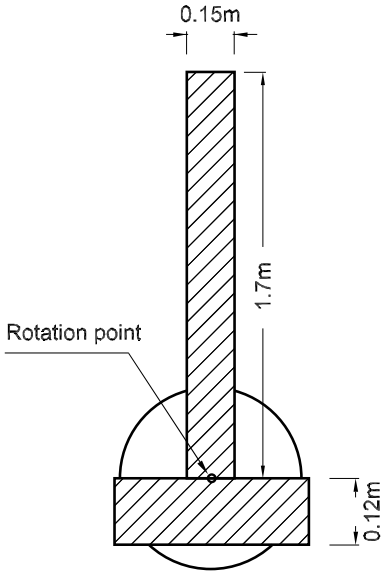


Figure A.3: Wheeled inverted pendulum.

**nertia of the wheel $I_w$**

Base on Figure A.2,

$$I_w = I_z = \frac{1}{2}mr^2 = \frac{1}{2}M_w r_w^2 = \frac{1}{2} \times 3.5kg \times 0.2^2 = 0.075kg.m^2$$

**Acceleration of gravity $g$**

$$g = 9.81m/s^2$$